



**Noble metal alloy complex nanostructures: Controllable synthesis and their electrochemical properties**

Journal:	<i>Chemical Society Reviews</i>
Manuscript ID:	CS-REV-12-2014-000478.R1
Article Type:	Review Article
Date Submitted by the Author:	30-Jan-2015
Complete List of Authors:	Wang, Xun; Tsinghua University, Liu, Huiling; Tsinghua University, Department of Chemistry Nosheen, Farhat; Tsinghua University, Department of Chemistry

## ARTICLE

# Noble metal alloy complex nanostructures: controllable synthesis and their electrochemical property

Cite this: DOI: 10.1039/x0xx00000x

Hui-ling Liu, Farhat Nosheen and Xun Wang\*

Received 00th January 2012,  
Accepted 00th January 2012

DOI: 10.1039/x0xx00000x

[www.rsc.org/](http://www.rsc.org/)

Noble metal nanocrystals have been extensively utilized as promising catalysts for chemical transformations and energy conversion. One of their significant applications lies in electrode materials in fuel cells (FCs) owing to their superior electrocatalytic performance towards the reactions both on anode and cathode. Nowadays, tremendous efforts have been devoted to improve the catalytic performance and minimize the usage of precious metals. Constructing multicomponent noble metal nanocrystals with complex structures provides the opportunities to approach the goal due to their highly tunable compositions and morphologies, leading to the modification of the related electrochemical properties. In this review, we first highlight the recent advances in the controllable synthesis of noble metal alloy complex nanostructures including nanoframes/nanocages, branched structures, concave/convex structures, core-shell structures and ultrathin structures. Then the effects of the well-defined nanocrystals on the modified and improved electrochemical properties are outlined. Finally, we make a conclusion with the points on the challenges and perspectives of the controllable synthesis of noble metal alloy complex nanostructures and their electrocatalytic performance.

## 1. Introduction

In the 18th century, Watt invented the steam engine and the initial power source of human beings and animals was changed to steam produced by burning coal. Since then, increasing amount of fossil fuels has been exploited to provide power for industrial manufacture and social development. However, the resulted environmental problems and accelerated depletion of fossil fuels requires the development of green and sustainable technologies on chemical transformations and energy conversion. In recent years, noble metal nanocrystals have been demonstrated as promising materials that may greatly contribute to solve the above issues due to their superior catalytic performance especially the energy-based electrochemical properties.<sup>1</sup> And according to their activities towards the reactions including hydrogen or organic small molecules electro-oxidations and oxygen reduction, noble metal nanomaterials have been widely used in FCs based on these reactions.<sup>2, 3</sup> Improving their electrocatalytic performance and

minimizing the usage of precious metals are still a major task for a long time to realize the commercialization of noble-metal-based FCs.

The catalytic performance of a catalyst includes activity, selectivity and stability. And there are three effects including ensemble effect, electronic effect and geometric effect, mainly influencing the catalytic performance of noble metal materials.<sup>4</sup> For ensemble effect, if a catalyst consists of multiple metals, multiple reaction sites are usually created. The multiple reaction sites can provide more opportunities to form appropriate binding configurations for a reactant molecule or intermediate, which could potentially facilitate the catalytic reaction.<sup>5, 6</sup> In the case of electronic effect, the electronic structure of catalyst surface can be modified through the electronic charge transfer between different components, leading to the modification and improvement of catalytic performance.<sup>7, 8</sup> Thirdly, geometric effect also has an influence on the catalytic performance. As in core-shell structures, the lattice mismatch between core and shell could make the strain arise. The strain could indirectly influence the electronic structure of the surface, then changing the catalytic results. Based on these aspects, constructing noble metal alloy complex nanostructures is necessary and could reasonably improve their catalytic performance.

Department of Chemistry, Tsinghua University, Beijing, 100084, P. R. China.  
E-mail: wangxun@mail.tsinghua.edu.cn; Fax: +8610 62792791;  
Tel: +8610 62792791, Prof. X. Wang

Nanocrystals with different morphologies can expose different facets, leading to different atomic arrangements on the surface. The various patterns on the facets result in distinct electronic and geometric structures, thus modifying the catalytic performance.<sup>9-11</sup> What's more, in this review, besides considering the multimetallic feature as complexity, the concept of "complex structures" is also compared with the traditional structures such as simple nanospheres, cubes and octahedra solely enclosed by {100} facets and {111} facets respectively. Thus we tend to emphasize the special morphologies including nanoframes/nanocages, branched structures, concave/convex structures, ultrathin structures and multicomponent and multi-layered core-shell structures as complex features. Such complex structures usually exhibit better catalytic performance due to their promising structural features. For example, when solid rhombic dodecahedral nanocrystals enclosed by {110} facets are fabricated as catalysts, the exposure of catalytic noble metals on the surface compared with the overall atoms is greatly limited. While through constructing complex structures, it can be reasonably solved. For instance, Xie's group successfully synthesized excavated rhombic dodecahedral PtCu<sub>3</sub> structures constructed by ultrathin nanosheets with the thickness of 2 nm.<sup>12</sup> Compared with the solid rhombic dodecahedral nanocrystals, the active facet is same, while the utilization of Pt atoms was significantly improved due to the ultrathin feature. And Yang's group constructed Pt<sub>3</sub>Ni nanoframes from solid rhombic dodecahedrons and obtained dramatically improved catalytic performance.<sup>13</sup> After systematic characterization, the optimized electronic structure on the surface of the arms of the nanoframes resulting from the combination of ligand effect and geometric effect intrinsically improved the catalytic performance of the materials. Moreover, the special morphology of 3-dimensionally accessible frames further endows the exposure of the optimal surface to a large extent. These results clearly demonstrate the effectiveness of complex structures to enhance their properties. Thus controllable synthesis of noble metal nanostructures is crucial to investigate the structure-dependent properties and design promising catalysts.

Among the numerous established synthetic systems towards nanocrystals, colloidal chemistry method is still considered as one of the effective and low-cost methods.<sup>14-16</sup> With this method, the structures of nanocrystals can be controlled both through thermodynamic and kinetic factors. The thermodynamically stable phase of noble metals is face-centered cubic (fcc) symmetry which favors the formation of highly symmetric shapes enclosed by low-index facets based on their intrinsic growth habits. To fabricate the above-mentioned complex structures, the isotropic growth needs to be broken. And the controllable synthesis of noble metal alloys is more complicated because of the distinct reduction potentials and nucleation/growth habits of different metals. However, from another perspective, it provides more opportunities to develop innovative structures.

In this review, we tend to summarize the recent achievements of controllable synthesis of noble metal alloy complex nanostructures and discuss the key factors behind the well-designed strategies. Then we review the structure-related electrocatalytic performance. Although several high quality reviews on noble metal nanomaterials have been delivered,<sup>17-19</sup> the review of recently developed complex structures has not been contributed. In this review, we mainly provide the discussions along the topic of complex features. We believe the efforts made in this review can pave the way to develop next-generation of electrocatalysts and realize the commercialization of noble-metal-based FCs.

## 2. Controllable synthesis of distinct complex nanostructures

### 2.1 Nanoframes/nanocages

Owing to their high specific surface area, open structures, large void space and potentially highly active sites on the maintained framework, nanoframes crystallized from noble metals have been demonstrated as effective catalysts by recent high quality references. In the past, many hollow structures have been synthesized and focused<sup>20-22</sup> but complex nanocage and nanoframe structures especially alloy nanoframes have not been kept under consideration. To obtain the nanoframes with precise size, open structure, three dimensionally accessible surfaces, controlled thickness and stable shell is a difficult task. Recently, some groups have synthesized and focused on the controlled synthesis of alloy nanoframes at the atomic level because of their improved electrocatalytic activity and durability. We plan to summarize the latest achievements on such materials and discuss the growth mechanisms including selective erosion, galvanic replacement and others in this section. In the past, numerous researchers have synthesized single component noble metal nanoframes/nanocages<sup>23-28</sup> but fewer had paid attention towards the synthesis of noble metal alloy nanocages and nanoframes for the purpose of electrocatalysis. Recently, these unique structures have been concerned and currently become the most appealing in the field of catalysis and electrocatalysis.

Chemical etching/corrosion or erosion can be manipulated to selectively remove definite facets of nanocrystals and the unstable metals from alloys coupled with the readjustment of remaining atoms to control the size, shape, composition and porosity of nanocrystals by the control of etchant strength and reaction environment. Considering the above features, it is an obvious route to construct open structures with three-dimensional surface accessibility. However, chemical etching has some shortcomings. For example, the surface atoms of alloys may be etched out in random sites and the etching process is usually too strong and difficult to control, and it may destroy the structures. Previously, numerous etchants have been used to synthesize the hollow or cage/frame structures including NH<sub>4</sub>OH or Fe(NO<sub>3</sub>)<sub>3</sub>,<sup>29</sup> Fe<sup>3+</sup>/Br<sup>-30</sup>, H<sub>2</sub>O<sub>2</sub>,<sup>31</sup> Cl<sup>-</sup>/O<sub>2</sub>,<sup>32</sup>

etc. It is a great challenge to control and moderate the etching process, and still more efforts are needed to find the ways to select a suitable etchant for the corrosion process. Additionally, complex structures obtained by the etching process also depend on the element-specific anisotropic distributions. Thus the compositional anisotropic distribution of different elements on the edges/corners and facets is related to geometrical anisotropy.<sup>33</sup> Most recently, an effective two-phase approach has been developed by Li et al.<sup>34</sup> in which the PtNi<sub>10</sub> nanoctahedra were corroded to Pt<sub>4</sub>Ni nanoframes. A “synergetic corrosion” mechanism was suggested in this instance in which several species (i.e., O<sub>2</sub>, H<sub>2</sub>O, H<sup>+</sup>, OAm, and EDTA<sup>4-</sup>) were involved. And OAm could play vital role in dispersion as well as in corrosion by coordinating with Ni<sup>2+</sup>. It was observed that the less and more amount of EDTA-2Na generated PtNi<sub>4</sub> porous octahedra and nanoframes respectively by influencing the corrosion rate. At last, the most significant feature of the two-phase process was controlling the corrosion reaction under mild conditions with an accelerated rate. In this system an aqueous phase in the presence of EDTA-2Na caused the obvious enhancement in corrosion to generate the PtNi<sub>4</sub> nanoframes. Recently, Stamenkovic and co-workers<sup>13</sup> presented an erosion method for the fabrication of Pt-rich Pt<sub>3</sub>Ni open-frame structure by preferential dissolution of Ni species followed by thermal treatment (Fig.1). The oleylamine-capped PtNi<sub>3</sub> polyhedra were firstly synthesized and then dispersed in non-polar solvents for two weeks at room temperature, which finally converted the nanocrystals into Pt<sub>3</sub>Ni nanoframes with three-dimensional molecular accessibility surfaces by interior erosion; by increasing the temperature of solution up to 120°C, etching time for complete nanoframes synthesis would be shortened from 2 weeks to 12 hours. Due to the rich distribution of Pt on the edges and more exposure of Ni on the facets (nickel could

with 2 nm thick edges. The formation of open frame structure with Pt-rich edges could be attributed to the anisotropic elemental distribution in the parent structure. Compared with other methods in which corrosion is conducted by harsh oxidizing agents or applied potential, in this protocol the erosion was carried out spontaneously by O<sub>2</sub> present in air and oleylamine in non-polar solvents. Thus the nanoframes with an open frame structure were produced and crystal surface chemistry was controlled efficiently with three-dimensional structure which increased the accessibility of reactants for both interior and exterior surfaces. Hollow Pt<sub>3</sub>Ni nanoframes could result from uneven distribution of Pt on the edges than that on their interior and the higher dissolution rate of Ni. However, sometimes etching and galvanic replacement reaction are coupled together in the one system. For example, Li et al. synthesized Pt-Ni nanoframes with Au islands and proposed a strategy based on the combination of selective galvanic replacement and priority-related chemical etching, in which the etching process has more prominent role in the nanoframes formation.<sup>35</sup> In the first step galvanic replacement between Au (III) and Ni (0) species started owing to the less electronegativity of Ni as compared with Au. It was predicted that the galvanic replacement reaction dominated at corners instead of edges and faces due to high surface energy and oxidized the nickel easily at the corners, thus producing top Au (0) atoms in solution, where Au islands were stacked on the Pt-Ni corners on the top of active nickel.

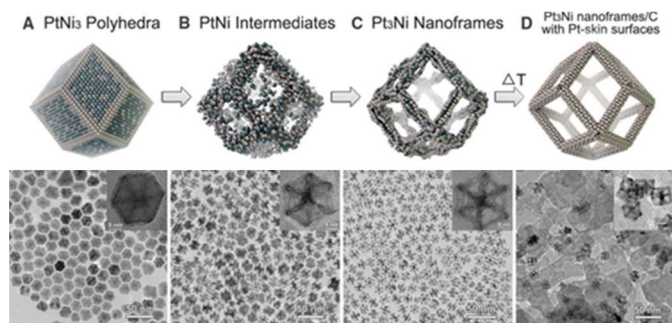


**Figure 1.** Schematic illustrations and analogous TEM images of the samples for the different stages during the evolution process from polyhedral to nanoframes. (A) Initial solid PtNi<sub>3</sub> polyhedra, (B) PtNi intermediates, (C) Final hollow Pt<sub>3</sub>Ni nanoframes, and (D) Annealed Pt<sub>3</sub>Ni nanoframes with Pt(111)-skin like surfaces disperse on high-surface area carbon. (Adapted with permission from ref. 13. Copyright 2014, American Association for the Advancement of Science).

readily form soluble complexes with oleylamine), the polyhedra were etched to form the open-framework Pt<sub>3</sub>Ni nanocrystals

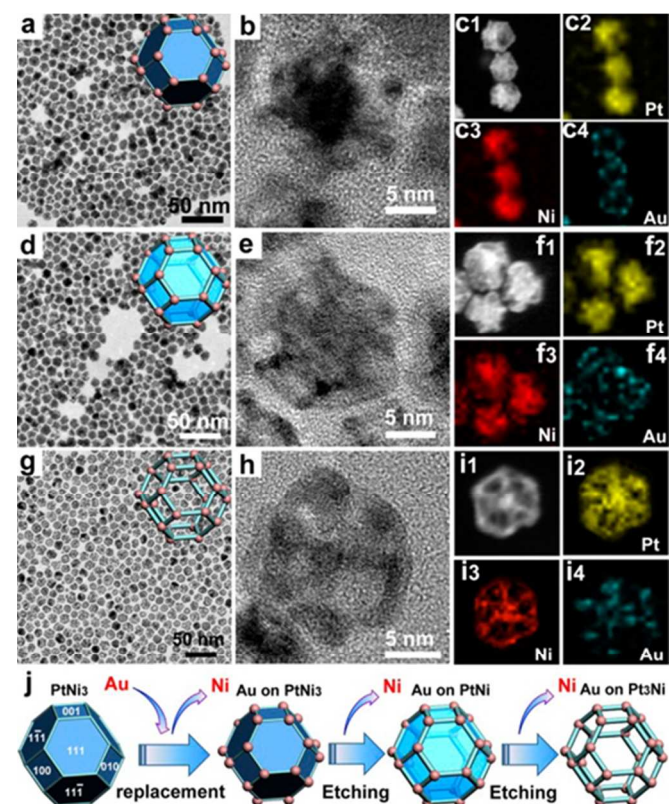


**Figure 2.** TEM images of (a) 10% Au on PtNi<sub>3</sub>, (d) 10% Au on PtNi, and (g) 10% Au on Pt<sub>3</sub>Ni. HRTEM images of (b) 10% Au on PtNi<sub>3</sub>, (e) 10% Au on PtNi, and (h) 10% Au on Pt<sub>3</sub>Ni. EDS elemental mapping images of (c) 10% Au on PtNi<sub>3</sub>, (f) 10% Au on PtNi, and (i) 10% Au on Pt<sub>3</sub>Ni. (j) Schematic illustration of the structural change from the truncated octahedral PtNi<sub>3</sub> to trimetallic hybrid Au islands on the Pt<sub>3</sub>Ni nanoframe (Adapted with permission from ref. 35, Copyright 2014, American Chemical Society).

The etching procedure was controlled by adding dimethylglyoxime, the non-vulnerability of Pt to dimethylglyoxime and strong Pt-Pt bonding interaction permitted Pt-protected nanoframes to be stable after etching. The second step involved structural priority related chemical etching during which the composition changed gradually from truncated octahedral PtNi<sub>3</sub> to 10% Au on PtNi<sub>3</sub>, to 10% Au on PtNi, and finally 10% Au on Pt<sub>3</sub>Ni by tuning the etchant amount as shown in Fig. 2. Lastly, this novel etching process controlled the Ni corrosion and Pt atoms distribution for the generation of nanosegregated Pt-skin edges with decorated Au atoms.

The galvanic replacement reaction is a simple and versatile route for the synthesis of complex nanostructures with tailored characteristics. It is a redox process, which involves the oxidation of one metal (commonly known as a sacrificial template) by the ions of another metal with a higher reduction potential.<sup>36</sup> The dissolution or oxidation of the metal occurs at the anode and the deposition or reduction of other metal ions would take place at the cathode. The most important factor for the galvanic replacement reaction is the difference in redox potentials of metals involved in the reaction system. Besides the composition, internal structure and morphology of nanocrystals could be controlled by tuning the order of metal salts addition, their amount and the shape of template, respectively. If the sacrificial template contains similar facets then the removal of template and deposition of atoms may happen simultaneously on all the facets. Conversely, if template has different facets then the galvanic replacement reaction may proceed with facet selectivity. The dissolution will start from high surface energy facets and deposition of fresh atoms will occur on low energy facets. The galvanic replacement reaction either carried out by using the template or by one-pot method (insitu formed template). Comparatively lower reduction potential of Ag than that of other metals like Pd, Pt and Au make its removal easy through the galvanic replacement reaction therefore Ag had been mostly used as a sacrificial template to fabricate hollow structures. For instance, by galvanic replacement reaction El-Sayed et al.<sup>37</sup> have synthesized Au-Pt, Au-Pd, Pt-Pd, Pt-Au, Pd-Pt, and Pd-Au double shell nanocages (the exterior shell composed of the first metal) with different sizes and controlled double shell thickness by using the silver as template. However, clean template surface, lattice mismatch and proper capping agents are important factors for the controlled synthesis. Furthermore, the shell thickness can be controlled by varying the amount of metal precursors. Instead of using silver template, Pd nanocrystals have also been used as sacrificial templates for the synthesis of Pd-Pt hollow nanocages by the coexistence of

galvanic replacement reaction and co-reduction. The co-reduction rate and galvanic replacement both should be carefully controlled to get the desired structures. Based on this, Xia and co-workers synthesized the Pd-Pt alloy nanocages with hollow centers by the combination of galvanic replacement between Pd nanocubes (sacrificial template) and K<sub>2</sub>PtCl<sub>4</sub> with a co-reduction method in the presence of citric acid.<sup>38</sup> In this case, high concentrations of Br<sup>-</sup> and PtCl<sub>4</sub><sup>2-</sup> ions, with a high temperature might accelerate the galvanic replacement and thus promote the formation of Pd-Pt alloy nanocages (Fig. 3a, b). Likewise, by substituting the citric acid with ascorbic acid, Pd-Pt nanodendrites were obtained due to rapid depletion of Pt precursor and decreased rate of galvanic replacement reaction. Similar galvanic replacement reaction has also been manipulated by Han and co-workers to synthesize Pd-Pt alloy octahedral and cubic nanocages with hollow interior and porous walls by using Pd octahedral and cubic nanocrystal as sacrificial templates, respectively.<sup>39</sup> The extent of galvanic replacement was controlled by changing the amount of reducing agent like ascorbic acid to get the Pd-Pt alloy with different morphologies. For example, higher and the lower reductant amount produced different dendritic structures. While in the absence of reductant, hollow nanocages with porous walls were achieved (Fig. 3c, d). Some other groups also have synthesized nanocages/frames by galvanic replacement reaction.<sup>40-42</sup> As discussed above, sacrificial templates have been used in galvanic replacement reaction, comparatively, Li and co-workers<sup>43</sup> reported one pot

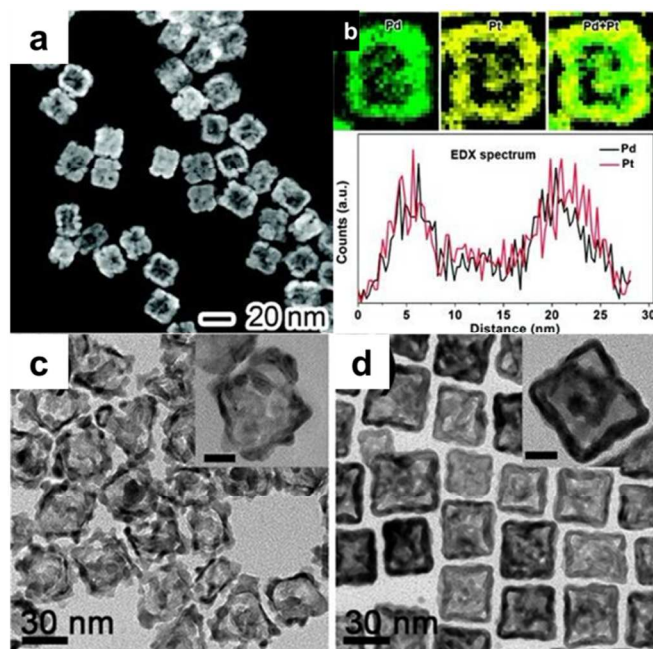


**Figure 3.** (a) High-angle annular dark-field STEM (HAADF-STEM) image of the Pd-Pt nanocages. The inset shows the high magnification HAADF-STEM image of single Pd-Pt nanocage; (b) EDX mapping (top) and line-scan (bottom) profiles of a single Pd-Pt nanocage; (Modified with permission from ref. 38, Copyright 2011, American Chemical Society); TEM images of (c) octahedral nanocages (ONCs); (d) cubic nanocages (CNCs), High-magnification TEM images are

shown in each inset. Scale bars in the insets indicate 10 nm (Modified with permission from ref. 39. Copyright 2012, American Chemical Society).

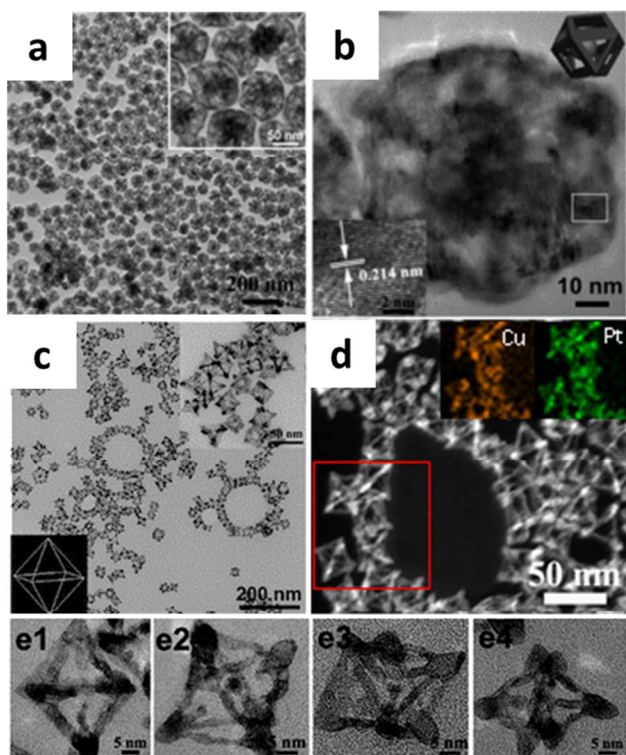
synthesis of Au-Ag octahedral nanoframes by the galvanic replacement reaction without using any template. The truncated polyhedral silver nanoparticles formed first in the solution. Then the selective gold deposition on the high-energy {110} surface in the presence of octadecylamine (ODA) and copper ions occurred. After this, diffusion and selective re-deposition of Au and Ag directed the formation of octahedral nanoframes with twelve sides and eight empty {111} facets. The presence of copper ions might boost the differences in growth rate of different facets. Additionally, the wall thickness and porosity could be controlled to a certain degree by controlling the size of the Ag nanoparticles.

To design bimetallic nanocrystals with complex structures in a one-pot method is more difficult than monometallic nanocrystals because the addition of second metal make the reduction kinetics more complex. The noble metals have higher standard reduction potentials (SPR) than non-noble metals, thus for the fabrication of alloy nanocrystals, the difference between the reduction potentials of two metals should be decreased. For this purpose, the reduction rates of two metals could be controlled by introducing the coordinating ligands in the reaction system. The reduction potential of metals can be reduced by complexation of metal cations with the powerful coordinating agents which could complicate their reduction. For example, halide ions could strongly coordinate to the noble metals and reduce their reduction potential.<sup>17</sup> Taking into account that the reduction potential of Pd<sup>2+</sup>/Pd (0.915 V) is more negative than that of Pt<sup>2+</sup>/Pt pairs (1.18 V) if the coordination

**Figure 4.** (a, b) TEM images of Pt-Cu yolk-cage alloy NCs. The top-right inset in a is the high-magnification TEM image; In (b), the top-right inset is the corresponding model image, and the bottom-left inset is the magnified HRTEM image taken from the selected area marked by rectangle; (Modified with permission from ref. 45. Copyright 2013, WILEY-VCH Verlag GmbH & Co. KGaA, Weinheim); (c) TEM image of as-prepared octahedral Pt-Cu nanoframes, the top-right inset shows a high-magnification TEM image of octahedral Pt-Cu nanoframes and the bottom-left inset shows the corresponding model image. (d) HAADF-STEM image of octahedral Pt-Cu nanoframes; the inset shows the selected-area (red rectangle) element analysis maps of Pt (green) and Cu (orange); (e1-e4) TEM images of an individual octahedral nanoframe with different orientations (Modified with permission from ref. 46. Copyright 2013, Royal Society of Chemistry).

environment is same, Zheng et al reported that the introduction of iodide ions to the mixture of [Pd(acac)<sub>2</sub>]/[Pt(acac)<sub>2</sub>] in the DMF solution could produce [PdI<sub>4</sub>]<sup>2-</sup> as the dominant precursor where Pd<sup>2+</sup> could reduce earlier than Pt<sup>2+</sup> ions.<sup>44</sup> For example, our group for the first time synthesized Pt-Cu alloy yolk-cage structure by glycine-mediated reduction kinetics.<sup>45</sup> It is worth noting that the shape and composition of nanocrystals can be controlled as well by varying the amount of glycine i.e. in this strategy glycine functioned as co-reductant and surface controller. Furthermore, glycine can coordinate with metal cations and in an aqueous medium glycine coordinated strongly with Pt<sup>4+</sup> instead of Cu<sup>2+</sup>, which favored the preferential reduction of Cu<sup>2+</sup>, although the standard reduction potential for Cu<sup>II</sup>/Cu (0.342V) is more negative than that of Pt<sup>IV</sup>/Pt pair (1.18V). Thus Pt ions reacted with reduced Cu nanocrystals via galvanic replacement reaction, leading to Pt-Cu yolk cage structure (Fig. 4a, b). In the same way, we also have synthesized single crystalline octahedral Pt-Cu nanoframes in which synergetic effect of hydroxyl and amine groups of ethanolamine and definite amount of glycine would affect the reduction rates.<sup>46</sup> (Fig. 4c, d). Likewise, cubic PtCu<sub>3</sub> nanocages have been synthesized by tuning the reduction rates by cetyltrimethylammonium bromide (CTAB) and the order of Pt and Cu species.<sup>47</sup> It was realized that the CTAB in oleylamine could act as co-reductant, and affect the reduction rates of Pt and Cu species so Cu ions could reduce before Pt ions although the copper pair has more negative reduction potential than Pt pair. It's seen that the coordinating ligands can change the reduction potential of metals and make the galvanic replacement reaction possible.

In addition to the above-described methods, cage/frame alloy structures also have been prepared by some other routes like kirkendall effect<sup>48</sup>, controlled decomposition kinetics<sup>49</sup> and long chain alcohol reduction process<sup>50</sup>. Furthermore, Ostwald ripening process has been used to create hollow interiors and porous surfaces with complex architectures<sup>51-53</sup>, thus this process could also be applied for the synthesis of noble metal alloy cages/frame structures. Generally, Ostwald ripening is a phenomenon in which small particles dissolve to minimize the



total Gibbs energy and redeposit onto the large crystal. To observe the Ostwald ripening process, one should carefully notice the change in crystal size which increases with the reaction time despite the composition remains unchanged. However, the present examples of the alloy nanoframes/nanocages rather than single metal ones fabricated by this method are still limited. Overall we can conclude that the etching is a more significant process for generating the open-frame structures with high-surface to volume ratio, and three dimensional active surfaces which improves the electrocatalytic efficiency by allowing the reactants to react with internal and external surfaces of nanoframes and the final morphology of nanocrystals mostly depend on the pattern of different elements how they are distributed. On the other hand, the galvanic replacement reaction can also be used to synthesize noble metal alloy nanocages/nanoframes with hollow interior, controlled porosity and thickness. Furthermore, still more investigations are required to control the erosion process and to find mild etchants which could retain the structural integrity and generate the open architectures.

## 2.2 Branched nanostructures

Noble metal alloy nanostructures with branched morphologies comprising dendrites, multipods and highly branched structures are fascinating for electrocatalytic reactions owing to their reasonably large surface area and potentially high active sites. It is a great challenge to synthesize an anisotropic noble metal structure as the noble metals favor to form face centered cubic (fcc) phase and lack the driving force for anisotropic growth. Thus, to make the structures anisotropically favorable it is important that the nuclei should be produced with defects like twin boundaries. Besides changing the seed structure, control of the reduction kinetics, selective binding interaction of capping agents, additives and other reaction conditions may induce the anisotropic growth. We will start our discussion with recent progresses in the synthesis of alloy nanostructures by the following synthetic routes: aggregation-based growth, seed mediated diffusion, anisotropic overgrowth, and etching process.

The aggregation-based crystal growth is a general path which may involve particle aggregation, attachment or diffusion for the synthesis of dendritic nanostructures. In this growth mode, smaller particles with high surface energy are produced in the nucleation stage through the fast reduction of metal precursors and aggregate or attach to each other to minimize the total surface energy. Generally, in this synthetic system control of the growth and attachment modes of metal nuclei are the key factors. Alloy dendritic structures could be synthesized by aggregation-based route in a one-pot method in which the in situ formed seeds act as nucleation sites for the further growth and no additional pre-synthesized seeds are required. The reduction rate is the most important parameter to efficiently control the nucleation and growth rates. In the current system, Chen et al.<sup>54</sup> reported a kinetically controlled co-reduction method for the synthesis of Pt-Cu alloyed nanodendrites. The

initial stage involved slow reduction in which the metallic species were reduced by ethylene glycol in air in the presence of additives such as FeCl<sub>3</sub> and HCl (mixture of additives and oxygen worked as an oxidative etchant). And the second stage was a fast reduction process, enhanced by the addition of ascorbic acid (AA). Moreover, the composition and size could be changed by varying the reaction time of the slow reduction step and the further coalescence of particles was controlled by the fast reduction step. Temporarily, growth kinetics can also be influenced by surfactants with different binding abilities which can change the growth modes of particles. In this report, by using oleylamine (OAm) and oleic acid (OA) as selective capping agents Li's group<sup>55</sup> synthesized Pt-Ni alloy nanodendrites through a one-pot solvothermal process. Here, the synergetic stabilization of

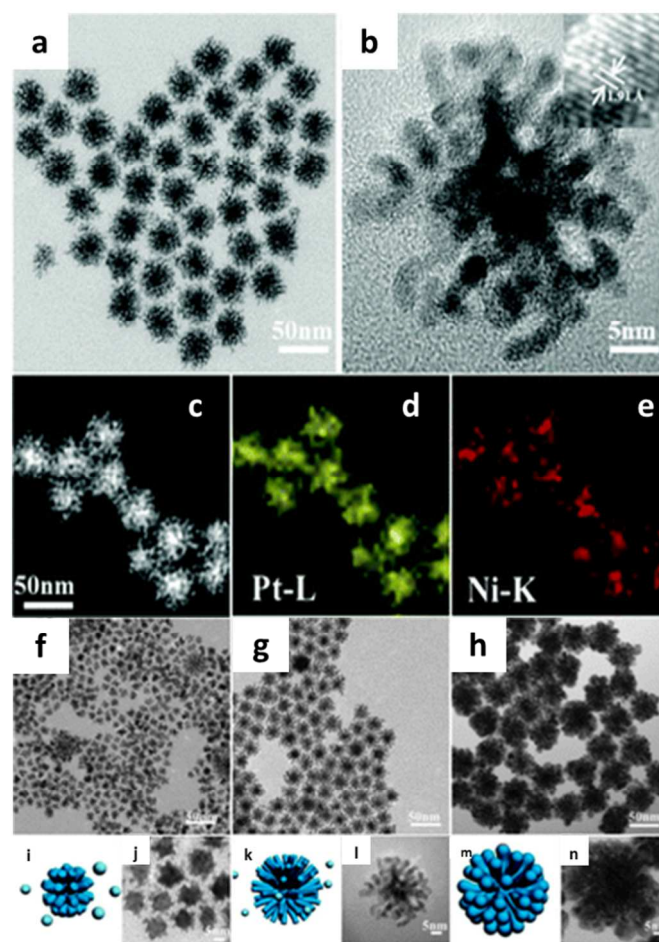


**Figure 5.** (a) TEM, (b) HRTEM, (c) HAADF-STEM images, (d) and (e) EDS mapping of bimetallic Pt-Ni nanodendrites. TEM images of Pt-Ni samples collected at (f and j) 100 minutes, (g and l) 120 minutes, (h and n) 480 minutes, (d, f and h) sketch maps of Pt-Ni samples collected at 100 min, 120 min, 480 min, respectively. (i, k and m) sketch maps of Pt-Ni samples collected at 100 min, 120 min, 480 min, respectively (Modified with permission from ref. 55. Copyright 2013, Royal Society of Chemistry).

two capping agents induced the anisotropic growth. Further observations illustrated that nanodendrites formed by rapid growth, initially small particles were produced, and then rapidly grew into dendritic structures as shown in Fig. 5. Thus, the selection of proper surfactants with selective binding abilities can change the growth kinetics by varying the rate of coalescence. Another group Feng et al.<sup>56</sup> also utilized this growth route to synthesize palladium-based bimetallic alloyed nanodendrites (PdM, M= Pt, Co, and Ni) by simultaneous reduction of metal salts in oleylamine (OAm) and hexadecylpyridinium chloride monohydrate (HDPC).

Besides the aforementioned processes, seeded-method coupled with the above route can also lead to the formation of nanodendrites with core of one metal attached by the branched arms of other metal. For example, Xia and co-workers<sup>57</sup> employed a heterogeneous seed-mediated method for the synthesis of a dense arrangement of Pt branches on a Pd core by directly reducing the  $K_2PtCl_4$  precursors with L-ascorbic acid. Although this is an effective aggregation based method to construct bimetallic branched nanostructure, nowadays this strategy has not been well extended to fabricate alloys, and thus more efforts should be devoted to this aspect. However, if branched seeds are used followed by the diffusion of another metal into the seeds to form alloy and the branched structure are well maintained, then the alloy branched nanostructures could be synthesized in this manner. In a typical instance, Li and co-workers<sup>58</sup> have fabricated such highly branched Pt-Ni nanobundles (NBs) with stepped surface by seed-based diffusion process. Pre-synthesized branched Pt nanocrystals were used as seeds to further generate the alloy Pt-Ni NBs by the diffusion of Ni into the seeds. The Pt-Ni NBs morphology was well inherited except with a minor increase in the branch width and length (Fig. 6). What's more, these highly branched alloy structures have rough surfaces containing high index facets.

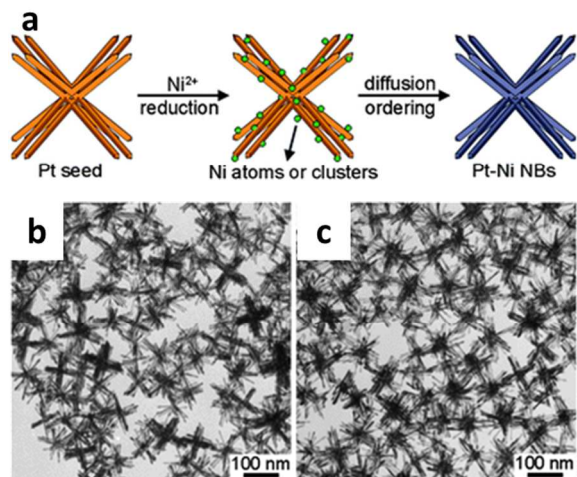


**Figure 6.** (a) Schematic illustration of the controlled synthesis of Pt-Ni nanobundles by a seed-based diffusion route. TEM image of (b) Pt seeds and (c) a randomly chosen Pt-Ni nanobundle (Modified with permission from ref. 58. Royal Society of Chemistry 2014).

Owing to their high surface energy with high surface area, branched multipod structures are not preferred thermodynamically and the growth under kinetic control should be conducted. When the growth rate is slow, the transfer of atoms to the crystal surface may take place in a relaxation manner to diminish the total surface energy and low-index faceted polyhedral nanocrystals may produce. While at the higher rate, an anisotropic growth may occur and the high energy facets form due to the higher rate of atoms addition than that of diffusion. Besides capping agent the rate of atom's addition and migration via diffusion on the seed surface could also determine the growth pattern and the structure of nanocrystals. Based on this approach, Zeng and co-workers<sup>59</sup> employed an aqueous method for the preparation of Cu-Pd multipods bound by low- and  $\{311\}$  high- index facets. In this process, metal precursors were reduced in the presence of glucose and capping agent octadecylamine (ODA). The decreased concentration of ODA induced an anisotropic growth due to its less binding and the increased level of atom's addition as a result multipods could be produced. While the more concentration of ODA could generate particles and polyhedron via diffusion due to less atom's addition to the nanocrystals. Later on, Li et al.<sup>60</sup> prepared bimetallic Pt/Cu hexapod concave nanocrystals which evolved from uniform Pt/Cu rhombic dodecahedron nanocrystals. The formation of hexapod structures involved three surfactants simultaneously. OAm has dual function as reductant and surfactant, didodecylmethyl-ammoniumbromide (DDAB) produced  $[PtBr_4]^{2-}$  and OA could act as a synergetic surfactant.

For the fcc metals to form an anisotropic structure, twinned seeds can also control the number and symmetry of branches. Recently, Hou and co-workers<sup>61</sup> proposed an aqueous synthetic method for pentacle Au-Cu alloy nanocrystals with fivefold twin planes. They used  $CuCl_2$  and  $H AuCl_4$  as metal source, glucose as the reducing agent and hexadecylamine (HDA) as the capping agent. In this process, initially symmetrical fivefold twinned decahedral seeds were formed, and then multiple branches projected parallel to the twinning planes. It was also investigated that the formation of definite pentacle nanocrystals might be hindered by the high or low amounts of capping/reducing agent producing polyhedral or rod like structures. Furthermore, the size of pentacle-shaped NCs was tailored by controlling the reaction time and the addition of capping agent (HDA). For example, less reaction time could reduce the size of decahedral seeds and injection of HDA might reduce the rate of reaction once the seeds formed and could promote the anisotropic overgrowth. Similarly by using the rod shape Au/Pd seeds with defects, Xu et al.<sup>62</sup> synthesized highly branched and symmetrical concave Au/Pd bimetallic NCs by using two surfactants simultaneously (e.g., CTAC and didecylmethylammonium bromide, DDAB). It was observed that synergistic effects of CTAC and DDAB in presence of  $AgNO_3$  could generate highly branched concave structures bound by  $\{411\}$  HIFs. The defects with twin planes could be produced in the excess of halides ions which cause the deposition of silver by under potential deposition mechanism

on Au at atomic steps, and then Pd/Au atoms further could adsorb on the twin planes owing to weak interaction of surfactants on these regions. Thus the stabilization by two surfactants may control the growth rate of the different planes producing the concave structures with spatially separated branched arms and increased surface area. Finally, it can be concluded that the growth kinetics and the twin structure of seeds both should be controlled well. To achieve this goal the addition of proper capping agent or additives is prerequisite.

Corrosion is a natural process and etching is one type of corrosion which could be employed as a synthetic method to construct the branched metal nanostructures. In this process combination of  $O_2$  in the air with halide ions may function as oxidative etchant and produce highly branched structures. For the first time our group<sup>63</sup> has synthesized unique and complex 3D-hierarchical Pt-Cu alloy superstructures with interconnected branches (tetragonal, highly branched and dendritic structures) via a simple hydrothermal method in which the NaI and  $I_2$  that formed in situ induced the etching process (Fig. 7a-f). It is generally known that NaI could be oxidized to  $I_2$  by  $O_2$  in the air, especially under high temperature which can facilitate the

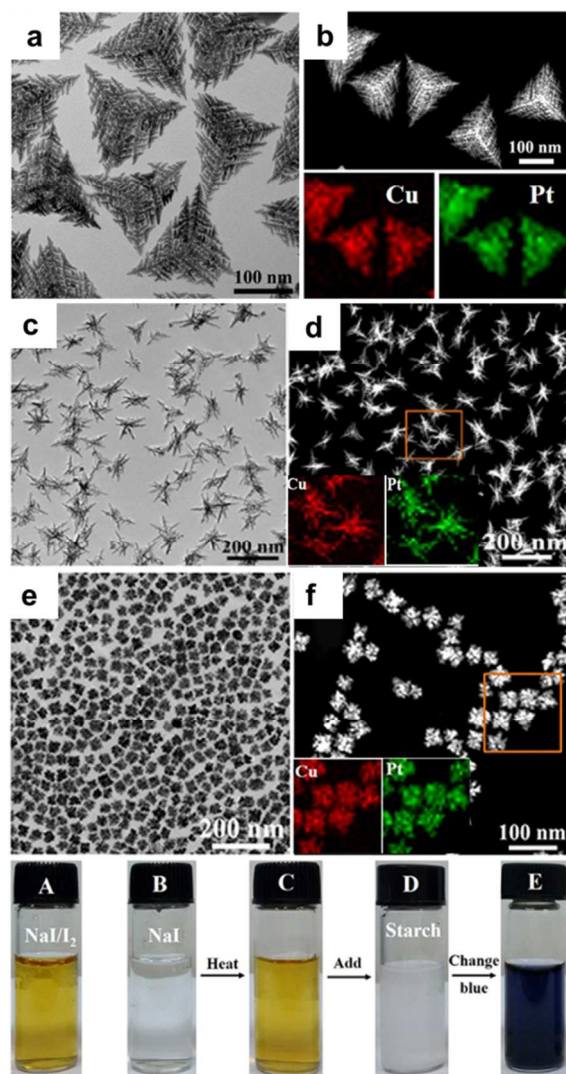


**Figure 7.** Images of Pt-Cu tetragonal, highly branched and dendritic superstructures: (a, c, e) TEM; (b, d, f) HAADF-STEM images, the red and green colors correspond to Cu and Pt elements; (A-E) Confirmation of the formation of  $I_2$  (the oxidation of  $I^-$  to  $I_2$  is revealed by the color change) (Modified with permission from ref. 63. Copyright 2014, Tsinghua University Press and Springer-Verlag Berlin Heidelberg).

oxidation of  $I^-$  to  $I_2$ . It was confirmed when the colorless NaI aqueous solution turned yellow on heating (Fig. 7B, C), and had the same color as a NaI/ $I_2$  solution (Fig. 7A), demonstrating that  $I^-$  can be oxidized to  $I_2$  by dissolved  $O_2$ . Furthermore, reaction between  $I_2$  and starch also confirmed the in situ formation of  $I_2$  (Fig. 7D, E). Additionally, it was found that by varying the amount of NaI the size, morphology, and crystallinity could be tuned, while the tryptophan played an important role in controlling the number and length of branches. Likewise, Tang and Chen<sup>64</sup> have reported the synthesis of Pt-Cu alloy nanodendrites by autocatalytic growth and selective oxidative etching, in which the absence of  $O_2$  did not produce dendrites. Thus, the selection of an etchant with suitable strength is a key point to get the nanocrystals with a preferred structures. For example, isotropic etching may occur in the presence of harsh etchant, while the nanocrystal's surface capped via surfactant could not be etched by weak etchants.

### 2.3 Concave and Convex Structures

Concave and convex structures of noble metal nanomaterials enclosed with high-index facets (HIFs) always exhibit attractive catalytic properties due to their high activities from their low-coordinated surfaces. However, synthesis of metal nanocrystals with high-index facets is a big challenge as these facets with high surface energies disappear rapidly during the crystal growth and show instability. This problem can be overcome by adding the capping agent or by kinetically controlled growth. During the growth process function of capping agent is preferential stabilization of low-coordinated facets of a seed. And in case of kinetically controlled growth, deposition of atoms could occur on the corners and edges. In the same way an appropriate amount of reductant is key to modulate the reduction kinetics. Meanwhile, by regulating the kinetics via surfactants, reducing agent, and metal precursors etc., high index faceted concave/convex NCs with different morphologies could be harvested. Since the synthesis of high-indexed tetrahedral Pt structures by Sun's group,<sup>65</sup> many efforts have been devoted to the preparation of concave and convex monometallic nanocrystals with high-index facets, but the exploration of noble metal alloy with complex convex and concave shapes has been increased in recent years because of their promising applications especially electrocatalysis. Hence, first we will discuss synthesis of concave nanocrystals by etching and galvanic replacement reaction.

An etchant with different etching abilities towards the different positions on nanoparticles could generate concave structures. The selective etching on the faces and edges coupled with overgrowth along the corners can produce concave

nanocubes, while the selective etching on the corners and edges would lead to the formation of multipods. Some monometallic concave nanocrystals have been reported by the selective etching<sup>66</sup>, but the synthesis of alloy concave nanocrystals is still a beginning. Recently, the coordination-assisted chemical-etching strategy was utilized by Li's group<sup>67</sup> for the preparation of well-controlled concave Pt-Ni alloys and chemical etching was regulated by the addition of coordinating complexes (dimethylglyoxime) at ambient temperature. Initially, the Ni atoms were oxidized to Ni<sup>II</sup> in the air. Owing to higher vulnerability and dissolution rate of Ni species than that of Pt, selective coordination of dimethylglyoxime to Ni<sup>II</sup> then could occur. As Fig. 8 explored that the concavity is enhanced with different phases of chemical etching in which the conversion of octahedron to round particles showed the initiation of etching process at the corners along the {100} direction. After the

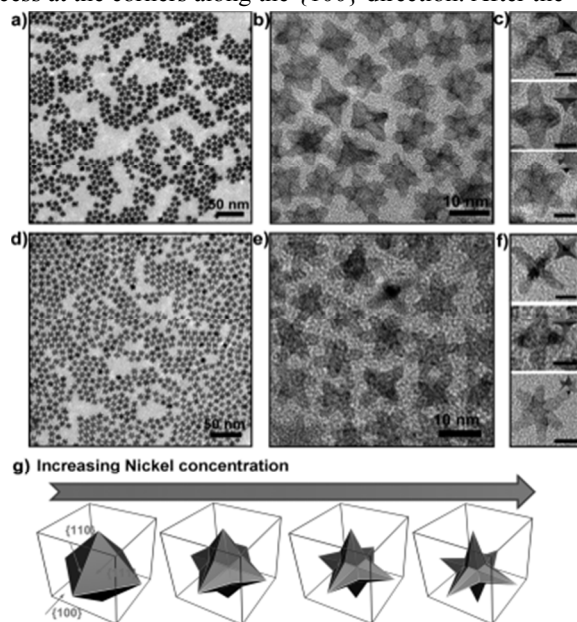


**Figure 8.** Shape evolution of octahedral PtNi<sub>10</sub> at different chemical etching phases a) 15 min, b) 30 min, c) 1 h, d) 3 h, e) 6 h, f) 12 h. Insets are the corresponding high resolution-TEM images with scale bars 5 nm (Modified with permission from ref. 67. Copyright 2012, WILEY-VCH Verlag GmbH & Co. KGaA, Weinheim).

formation of {100} facets, etching occurred at {110} and {111} directions. Finally, the facets and edges could be etched to curl the cavities leading to concave structures. Thus, different etching priorities on particular sites of nanocrystals could generate concave structures. In the absence of dimethylglyoxime, chemical etching could not happen even at higher temperature elucidating its importance in etching. Conversely, harsh etchants like concentrated HNO<sub>3</sub> would cause the structural breakdown and agglomeration. Consequently, selective etching can be further elaborated by understanding the depth of etching with controlled attack on the selective facets to generate the complex concave structures. Still, many significant trials are needed to synthesize the concave nanocrystals by etching process.

The galvanic replacement reaction is a general process for the synthesis of hollow structures, nanocages etc. However, the galvanic replacement reaction is also applicable to the synthesis of concave structures. In comparison to nanocages in which dissolution occurs at the corners of template first<sup>38</sup>, the formation of concave structure is directed through the dissolution of template from the middle side faces. Further, the size and shape of nanocrystals could vary according to the size and shape of templates used in the synthesis. Previously, bromide induced galvanic replacement reaction has been employed for the fabrication of bimetallic Pd-Pt concave nanocubes via using regular Pd cubes as seeds by Xia's group.<sup>68</sup>

In this case the preferential oxidation and dissolution of Pd atoms from the {100} facets of a Pd cube occurred along with the deposition of freshly formed Pt atoms on the {111} facets to

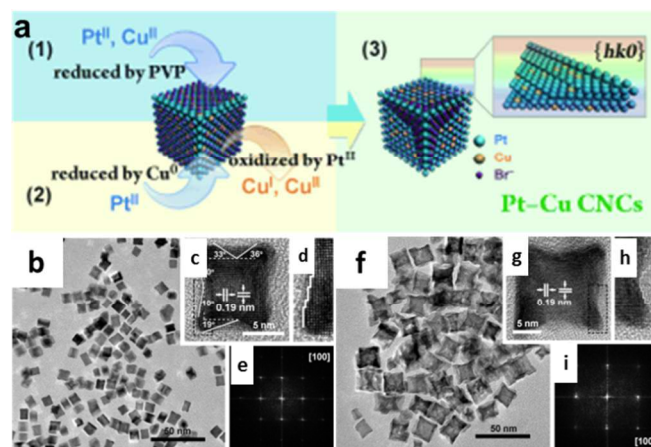


**Figure 9.** (a) Schematic illustration for the formation of Pt-Cu CNCs, TEM, HRTEM images and FFT patterns of Pt-Cu NCs (b-e) and Pt-Pd-Cu CNCs (f-i) (Modified with permission from ref. 70. Copyright 2012, WILEY-VCH Verlag GmbH & Co. KGaA, Weinheim).

form concave structures. Following the same strategy, Yang and co-workers<sup>69</sup> synthesized Pd-Pt alloy concave nanocubes enclosed by HIFs with variable compositions (from Pd<sub>40</sub>Pt<sub>60</sub> to Pd<sub>83</sub>Pt<sub>17</sub>). In the similar way, Yan and co-workers<sup>70</sup> prepared Pt-Cu and Pt-Pd-Cu concave cubic alloy nanocrystals (CNCs) with different compositions by modulating the reaction kinetics and the galvanic replacement process. The Pt<sup>II</sup> and Cu species, Br<sup>-</sup> and H<sup>+</sup> ions were essential to the formation of CNCs. In this process, initially seeds formed in solution on which the galvanic replacement reaction between Pt<sup>II</sup>, Cu<sup>II</sup> species and reductive PVP would take place. After that irregular polyhedrons formed by the selective passivation of Br<sup>-</sup> ions on {100} facets, then galvanic reaction occurred between reduced Cu<sup>0</sup> atoms of the nanocrystals and oxidative ions like [PtBr<sub>4</sub>]<sup>2-</sup>, H<sup>+</sup> from the solution. Finally, [PtBr<sub>6</sub>]<sup>2-</sup> preferentially oxidized and dissolved the Cu atoms on the {100} facets due to their higher concentration near corners where diffusion of electrons in the Pt-Cu crystals reduced the all Pt/Cu (II) species, and deposition of these atoms on the corners or edges of NCs

directed the formation of concave nanocubes with high index steps (Fig. 9).

For the synthesis of concave structure crystals, facets growth can be controlled by capping agent owing to the change in surface energies and which may also change the crystal growth kinetics according to their binding strengths. Thus, the selection of an appropriate capping agent with selective binding ability is important to get the alloy concave structures with desired facets. For instance, Fang et al.<sup>71</sup> synthesized concave Pt<sub>3</sub>Co nanocubes with HIFs. The synthetic process was carried out by the nucleation (dependent on the concentration of free metal atoms) followed by anisotropic overgrowth and protection of high-index planes by controlled binding of oleylamine (OAm)/oleic acid (OA). As OAm and OA could exhibit different binding capabilities on different facets. In this system, crystal growth along {100} plane was inhibited due to a relatively high ratio of OAm/OA, thus the selective binding of OAm/OA could change the surface energy on each facet, and the resultant anisotropic overgrowth could construct concave nanocubes. Similarly, by introducing the different concentrations of capping agent octadecyltrimethyl ammonium chloride (OTAC), Au-Pd alloy nanocrystals have been fabricated systematically with the shape change from rhombic dodecahedral (RD) to trisoctahedral (TOH), and hexoctahedral (HOH) structures with the almost similar size and composition by Zheng et al.<sup>72</sup> The formation of high index facets and morphology changes could be attributed to the capping agent as well as the kinetically controlled crystal growth by the increased reduction rate. In addition to capping agents, metal ions may also influence the growth rate of nanocrystals through binding interaction to the surfaces of nanocrystals. Recently, Yang et al.<sup>73</sup> illustrated an oil-phase methodology for Pt-Cu alloy concave nanocubes with high-index facets. The variation in precursor's ratio changed the reduction process consequently altering the growth rate. The higher ratio of Pt<sup>2+</sup> produced multipods owing to the selective overgrowth on the {111} plane as a result of its fast reduction rate. Conversely, reduced Pt<sup>2+</sup> ratio could retard the reduction rate leading to concave cubes formation via surface diffusion from corners to edges. Further, detailed observation showed that the under potential deposition (UPD) mechanism associated with Cu<sup>2+</sup> might involve in the production of high-index facets by stabilizing the low-coordination sites. Actually, the UPD is a mechanism in which the potential of electro-deposition of metal monolayer on another metal surface can be lower than that of the deposition on the same metal surface. In this context, Zheng et al.<sup>74</sup> also synthesized hexoctahedral (HOH) Au-Pd alloy NCs encased with 48 {431} high-index facets with assistance of under potential deposition (UPD) of Cu on Au which induced simultaneous reduction of Au and Pd. In addition to formation of high index facets, Cu<sup>2+</sup> UPD also facilitated the alloy formation (Fig. 10 a). Alternatively, the growth rate can also be manipulated by the addition of glycine. Very recently, Sun et al.<sup>75</sup> have prepared the Pt-Ni alloy nanocrystals with different morphologies i.e. concave nanocubes (CNCs), cubes and hexoctahedra (HOHs) by tuning the glycine amount which

modulated the nucleation and growth rates of the Pt-Ni alloy structure (Fig.10b, c and d1-d4).

Besides the overgrowth process for the concave and convex nanocrystals which include facet selective capping and kinetic control growth without any template or seeds. Through seed-mediated growth method, many researchers have reported the convex/concave core-shell structures with different shapes and high index facets by using Pd seeds<sup>76-78</sup> and Au seeds<sup>79-82</sup> but few groups have synthesized alloy NCs with this method.<sup>83</sup> In this review, our main focus is alloy nanostructure, therefore, we didn't present detailed description in this regard. As a whole, kinetically control growth together with a capping agent were found to be useful and emerging protocols to the generation of well-defined concave/convex shapes and high index facets.

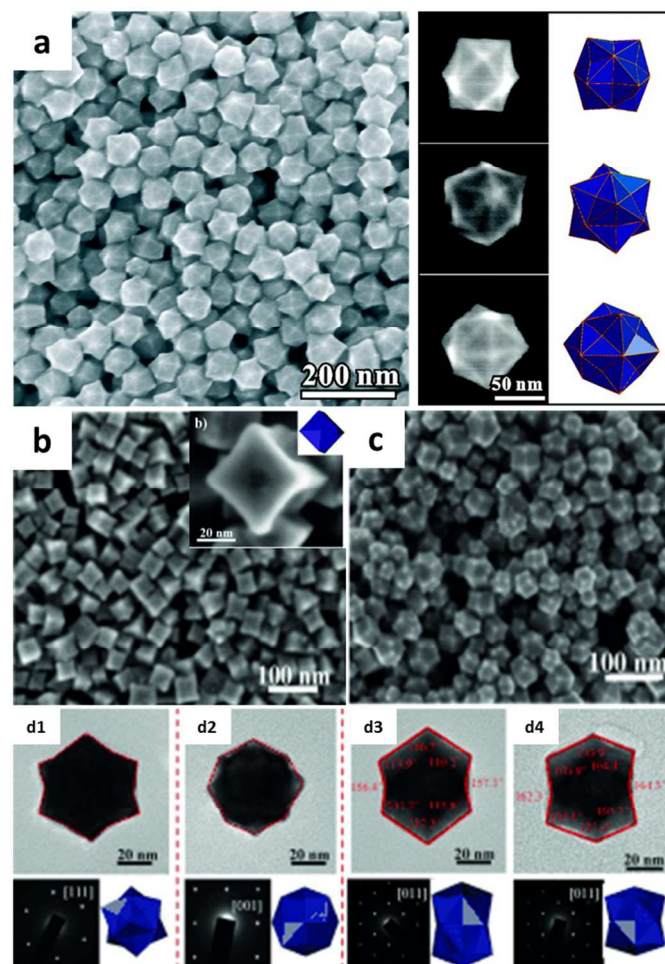


**Figure 10.** (a) SEM image of the as-prepared HOH Au-Pd alloy NCs with a series of high-magnification SEM images and corresponding models images (Modified with permission from ref. 68. Copyright 2011, American Chemical Society); (b) SEM, HRSEM and corresponding model of Pt-Ni alloy CNCs, (c) SEM image and the TEM image with corresponding SAED patterns and structural models of the HOH Pt-Ni alloy NCs viewed along the [111] (d1), [001] (d2), and [011] directions (d3-d4) (Modified with permission from ref. 75).

Copyright 2014, WILEY-VCH Verlag GmbH & Co. KGaA, Weinheim).

#### 2.4 Ultrathin nanostructures

Actually, a strict definition of ultrathin nanostructures has not been clearly established. Previously, the size of sub-10 nm has always been pronounced as the feature of ultrathin and described with the term of ‘several nanometers’.<sup>84, 85</sup> While with the fast-growing development of synthetic methods of nanomaterials, the size of at least one dimension of nanocrystals has been constantly decreased.<sup>86</sup> In this review, we tend to refer to the ultrathin nanocrystals with further decreased dimension to sub-5 nm or even 1 nm. Recently, our group has discovered that 1 nm maybe a critical size to observe some interesting phenomenon such as polymer-analogous properties<sup>87</sup> and unique DNA-like assembly behavior<sup>88</sup> in the world of inorganics. Nowadays, ultrathin noble metal nanocrystals have been demonstrated to possess numerous extraordinary properties.<sup>86, 89</sup> Especially as electrochemical catalysts, the ultrathin structures can potentially provide high specific surface area and consequent promising catalytic performance. Thus tremendous efforts have been devoted to synthesize ultrathin noble metal nanocrystals. While compared with metal oxides, metal sulfides and metal hydroxides with ultrathin structures, the achievements in noble metal materials are still limited. In this subsection, we highlight the recently developed methods for the synthesis of noble metal alloy nanocrystals with ultrathin structures. According to the following discussions on their electrocatalytic properties, tiny metal clusters are not involved in this part.

One dimensional (1D) noble metal nanomaterials have attracted extensive interests owing to their applications in a wide range of fields.<sup>90-92</sup> To obtain such structures, their favorable isotropic growth mode should be broken and the growth direction should be confined along one certain direction with the other two inhibited directions. And to further confine the diameters in ultrathin region, specific capping agents and surfactant ligands are usually needed to control the growing process and simultaneously stabilize the high energy surface on formed ultrathin nanostructures. Recently, the developed template mediated and oriented attachment routes have been successfully utilized to fabricate ultrathin noble metal alloy nanowires. Hard templates such as porous anodic aluminum oxide<sup>93</sup> and mesoporous silica<sup>94</sup> have been extensively used to confine the shapes of nanocrystals, while the movement of the templates is always needed as post treatment. For ultrathin nanocrystals, the post treatment would readily destroy the formed nanostructures. Recently, special sacrifice templates such as ultrathin Te nanowires have been for the first time developed by Yu’s group to come over this drawback and successfully synthesize 1D noble metal nanostructures.<sup>84</sup> Through galvanic replacement reaction between ultrathin Te nanowires and noble metal precursors, Te element is totally replaced and the high-quality ultrathin structures are well inherited. Due to the effectiveness of this method, Dong et al.

further used Te nanowires to synthesize PdM (M= Pt, Au) bimetallic and AuPtPd trimetallic alloy nanowires.<sup>95, 96</sup> Although the diameters are around 10 nm, it is believed as a promising strategy for further development to synthesize ultrathin structures. Besides the hard-template mediated method, soft templates have also been demonstrated as desired materials to synthesize ultrathin nanostructures.<sup>97, 98</sup> In this method, surfactants with hydrophilic tips and hydrophobic chains are always utilized as the building blocks to form soft templates in liquid solutions. And metal precursors are coordinated and reduced in the chambers of the micelles, i.e., the soft templates. Thus, it is obvious that the shapes of the initially formed templates are crucial to control the final morphologies of nanocrystals. To obtain 1D ultrathin nanostructures, the chambers should hold the above-mentioned ultrathin feature and confine the growth of nanocrystals along a certain direction. Many factors such as concentration and structure of the surfactants, solvent system and reaction temperature have an influence on the formation of soft

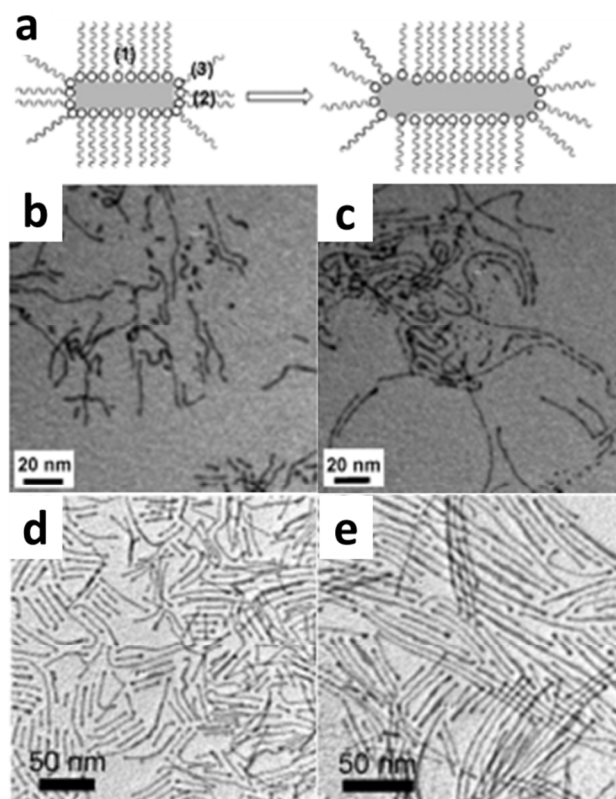


**Figure 11.** (a) Schematic illustration of the growth of FePt nanowires/nanorods; (b, c) TEM images of the FePt nanorods/nanowires obtained from the reaction in oleylamine at 120 °C for 2 min and 5 min, respectively. (Adapted with permission from ref. 99. Copyright 2007, WILEY-VCH Verlag GmbH & Co. KGaA, Weinheim.) TEM images of (d) 2.5 nm wide Fe<sub>56</sub>Pt<sub>44</sub> and (e) Co<sub>63</sub>Pt<sub>37</sub> nanowires. (Modified with permission from ref. 101. Copyright 2013, WILEY-VCH Verlag GmbH & Co. KGaA, Weinheim.)

templates. The structure of the surfactants directly determines the properties of the soft templates. With chosen surfactants, the formation of templates needs a critical concentration. Templates with steady shapes can't form under the value, while the templates will become bigger and aggregate at high concentration. The solvent system determines the property of the templates, i.e., hydrophobic or hydrophilic interior environment. The reaction temperature can influence the values of the mentioned critical concentration. Recently, a series of organic acids and amines with long carbon chains have been mainly used to effectively construct the soft templates and fabricate ultrathin noble metal alloy nanowires. Typically, Sun's group reported the successful synthesis of ultrathin FePt nanowires with a diameter of ~2 nm by thermal decomposition of  $\text{Fe}(\text{CO})_5$  and reduction of  $\text{Pt}(\text{acac})_2$  (acac=acetylacetonate) in the presence of OAm and octadecene (ODE).<sup>99</sup> OAm molecules were introduced in this system to act as weak reductant and the building blocks of soft templates. They claimed that OAm formed elongated reverse-micelle-like templates, and the different OAm capping densities on the micelle surface controlled the growing direction and diameter of the nanowires. As shown in Fig. 11a, the dense and well-organized side capping in area (1) inhibited the growth along this direction and the loosely packed tip areas (2) and (3) led to the addition of precursors and elongation of the nanowires. TEM images in Fig. 11b and 11c exhibited the elongation process under prolonged reaction time. Interestingly, the lengths of the ultrathin nanowires could be tuned by modifying the OAm/ODE ratio. Later, they combined this effective strategy with galvanic replacement to fabricate ultrathin FePtPd nanowires by reducing  $\text{Pd}(\text{acac})_2$  with Fe atoms in the above-mentioned FePt nanowires<sup>100</sup> and made a modification of the discussed method to synthesize ultrathin FePt and CoPt nanowires<sup>101</sup> (Fig. 11d and 11e). All the discussed results show that the diameter of the nanowires synthesized through soft-template mediated method is desirably uniform. The uniformity is resulted from the unique elongation mode by the confinement of soft templates.

Oriented attachment has also been demonstrated as a promising route to construct ultrathin nanowires. To drive the growth under this mode, precursors should undergo a boost nucleation and totally form nuclei which then enter the attachment stage to decrease the total free energy. Since the final morphologies of nanocrystals formed through this mechanism are strongly dependent on the structures and oriented directions of the coalescence units, the formation of ultrathin nanowires requires mainly two points: (1) the size of the oriented units should be limited in the ultrathin region; (2) the units need the driving force to attach with each other along a certain direction for assembling into nanowires. In the synthesis of alloy nanowires, the compositions of different metals usually have a great influence on the attachment process and consequent morphologies of the final nanocrystals. In a typical example, Yang's group observed that the formation of ~3 nm Pt-Ag alloy nanowires strongly depended on the ratio of Pt/Ag.<sup>102</sup> A nearly equal amount of Pt and Ag was the optimal

condition. Through density functional theory calculation and molecular dynamic simulation, their results showed that the composition of initial units influenced the interaction between the binding energy of surfactants on alloy surface and the diffusion of metal atoms at the interface of attached tiny particles which determined the nanowires growth. Later, Li's group reported the synthesis of ultrathin 2nm Au/Ag nanowires under oriented attachment by reducing  $\text{HAuCl}_4 \cdot 4\text{H}_2\text{O}$  and  $\text{AgNO}_3$  with octadecylamine as the sole solvent.<sup>103</sup> In this system, both the reaction temperature and Au/Ag ratio were the key factors for the formation of ultrathin nanowires. Recently, they successfully obtained ~3 nm PtM (M=Cu, Co, Ni, Fe) alloy nanowires with different ratios by adjusting the amount of OAm used as surfactant.<sup>104</sup> In this case, the variety of the amount of surfactant mostly compensated the influence of the change of composition which promised a wide range of composition of the nanowires. Most recently, a novel synthetic system was designed by Wang and Lou et al. to fabricate Pt bundles of 3 nm nanowires in the presence of KOH and N, N-dimethylmethanamide (DMF).<sup>105</sup> They claimed that the reaction of KOH and DMF could produce amine species which adhered on Pt surface and directed the oriented attachment growth mode. This strategy was also effectively extended to synthesize Pt-Au and Pt-Pd alloy ultrathin nanowires. Different from the nanocrystals capped by surfactants with long carbon chains, the nanowires surface in this instance adsorbed small amines species which was desirable for the application as catalyst.

To date, the construction of ultrathin two dimensional (2D) noble metal nanomaterials still remains as a big challenge. The three-dimensionally close-packed structure of noble metals makes it difficult to form metal nanosheets with the thickness of only several atoms. While under the tremendous efforts to develop such materials, some achievements of the fabrication of ultrathin noble metal nanosheets with single component have been reported. In 2010, Zheng's group utilized CO as the confinement agent to restrict the thickness of Pd nanosheets to 10 atoms.<sup>106</sup> Ultrathin 2-nm thick Au nanosheets with a totally novel hcp crystalline structure were fabricated on the surface of graphene by Zhang's group in 2011.<sup>107</sup> Recently, single-atomic layered Rh nanosheets with a conjugated d-bonding framework were amazingly synthesized with PVP by Li's group and they named the structure as 'metallene'.<sup>108</sup> In these cases, CO, graphene and PVP are the crucial confinement agents. Besides the single component ultrathin nanosheets, the synthesis of noble metal alloys with such structure needs to overcome more difficulties due to the intrinsic different nucleation and growth processes of different metals. For the first time, our group established a two-step method to fabricate high-purity ultrathin Pt-Cu alloy nanosheets of 4-6 atom thickness.<sup>109</sup> In this system, a gel-like material was fabricated first and then was used in the second step to confine the formation of tiny nuclei and subsequent 2D growth mode. Potassium iodide played a key role to control the lateral sizes of the nanosheets from 10 nm to 50 nm as shown in Fig. 12a-c. Interestingly, the ultrathin nanosheets could curve to nanocones if trace amount of  $\text{H}^+$  was

added in the second step (Fig.12d). The curving behavior may derive from the ultrathin thickness which endows the nanosheets with flexible feature to some extent. Then we successfully modified this synthetic method to fabricate one-atom thick Pt-Cu alloy nanosheets.<sup>110</sup> Besides KI utilized in the former system, we further introduced ascorbic acid (AA) as a strong reducing agent which played a crucial role in the newly developed system. AA could effectively increase the nuclei at the beginning of reaction, controlling the thickness of the nanosheets in one-atom level and keeping their lateral size small. To our best knowledge, it is the first example of noble metal alloy nanosheets with the thickness of just one atom. Very recently, a complex structure constructed with ultrathin nanosheets was synthesized by Xie's group.<sup>12</sup> The fabricated PtCu<sub>3</sub> alloy nanocrystals owned unique excavated rhombic dodecahedral (ERD) structure which was constructed with 2-nm nanosheets exposing high-energy {110} facets as shown in Fig.12e-h. The investigation of the growth process indicated that n-butylamine was a crucial facet-specific capping agent which could stabilize {110} facets and decrease the growth rate of these facets. In the above-mentioned cases, the ultrathin feature facilitates the exposure of atoms on the surface to the largest extent, leading to an effective utilization of noble metals. While the synthesis of noble metal alloys with ultrathin 2D structures is still limited, innovative and effective strategies are highly desired to enrich the achievements of this respect.

### 2.5 Multicomponent and multilayered core-shell nanostructures

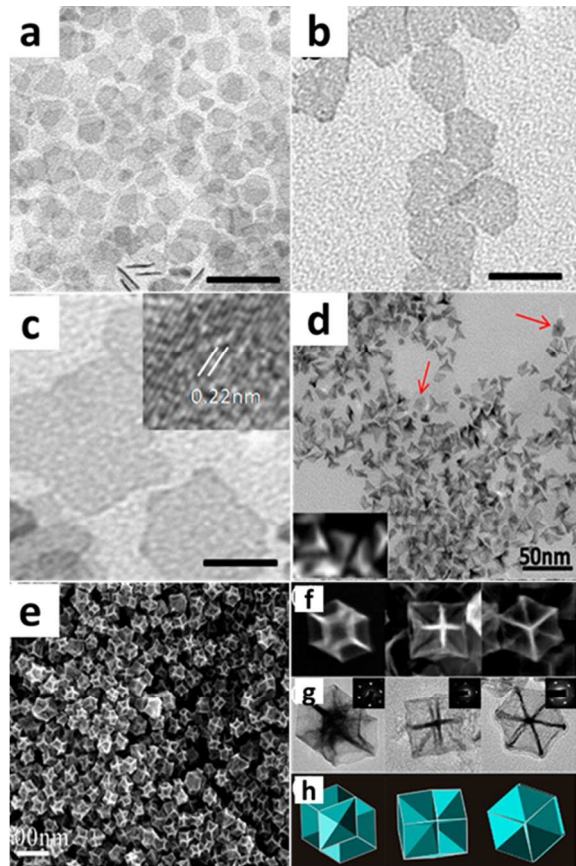


**Figure 12.** TEM images showing nanosheets of different size on increasing the amount of KI: (a) 10, (b) 20, and (c) 50 nm (inset corresponds to the visible lattice fringes; scale bars 20 nm). (d) TEM image of Pt-Cu nanocones (inset shows the HAADF image). (Modified with the permission from ref. 109. Copyright 2013, American Chemical Society.) (e) SEM image of the ERD PtCu<sub>3</sub> nanocrystals on a large scale. (f) SEM images and (g) High-magnification TEM images and (insets) the corresponding SAED patterns of an individual ERD PtCu<sub>3</sub> alloy nanocrystal with different orientations. (h) Schematic models of an ERD PtCu<sub>3</sub> alloy nanocrystal viewed along the [110], [100], and [111] directions. (Modified with the permission from ref. 12. Copyright 2014, American Chemical Society.)

Core-shell noble metal nanocrystals have been demonstrated as one kind of important electrocatalysts due to their distinct structural features and unique chemical and physical properties.<sup>111-113</sup> The structure of a core-shell nanoparticle can be highly designed through the modification of core, shell and the interface. Usually, the core with a different lattice constant from that of the shell can introduce lattice strain on the particle surface and bring geometric effect.<sup>4</sup> And under monolayer shell, the core can also introduce electronic effect through interaction with the surface atoms.<sup>114, 115</sup> The structure of shell directly influences the overall surface information. The variety of the structures can reasonably modify the related properties of core-shell nanoparticles. And from the economic point of view, constructing core-shell structures with an effort to minimize the usage of precious metals is also an effective strategy to meet the requirement for industrial applications of noble-metal-based electrocatalysts. Therefore, the realization of controllable synthesis of such nanocrystals with well-defined structures is of profound significance to investigate their structure-dependent properties and provide guidance to develop novel materials. Nowadays, numerous synthetic strategies have been developed to fabricate bimetallic core-shell nanostructures and some high quality reviews have already delivered the discussions.<sup>116, 117</sup> While further increasing their complexity through introducing a third metal or third layer is absolutely necessary to provide more opportunities to further tune their properties. For the development of next generation of electrocatalysts, the assemblage of multifunction in one catalyst is highly desirable. High complexity is expected to promise the realization of this respect. Therefore, we tend to emphasize the recent developments of the synthesis of more complex core-shell nanostructures with multimetallic components and multilayers in this subsection. The most effective route is seed-mediated growth which has been utilized to synthesize both multicomponent and multilayered core-shell nanocrystals. Besides, one pot coreduction synthetic method has also been discussed.

In the seed-mediated growth, seeds are usually fabricated first and then mixed with the shell metal precursors in the same pre-conducted system or in a different synthetic environment after purification. The growth of shell on preformed seeds is usually thermodynamically favored. Heterogeneous nucleation of shell metal is realized when its critical energy is lower than that of homogenous nucleation.<sup>118</sup> And there exist three typical

growth modes in the shell formation process: layered growth, island growth and intermediate growth, which is determined by the overall excess energy of the entire system. Lattice mismatch and interaction between the core and shell materials mainly determine the interfacial energy and consequent growth mode.<sup>119</sup> Through well-designed strategies based on the above principles, a series of multimetallic core-shell metal/alloy, alloy/metal and alloy/alloy structures have been synthesized. If a mixture of metals is deposited on preformed seeds, alloy shell can be constructed. Sun's group utilized Pd nanoparticles as seeds and then controlled the reduction of  $\text{Pt}(\text{acac})_2$  and decomposition of  $\text{Fe}(\text{CO})_5$  on Pd surface to synthesize core-shell Pd/FePt nanocrystals.<sup>120</sup> In this system,  $\text{Fe}(\text{CO})_5$  was confirmed to be crucial for the nucleation and growth of FePt on the surface of Pd seeds. And the reaction temperature, amount of  $\text{Fe}(\text{CO})_5$  and Pd seeds all influenced the final core-shell structures. High temperature was undesired because the consequent high reduction rate could break the equilibrium of shell formation step. Slow reduction rate under relative low temperature favored the layer growth mode. Then they extended this system to successfully synthesize a series of multimetallic core-shell nanomaterials including Au/FePt<sup>113</sup>, Au/CuPt<sup>121</sup> and Ag(Au)/CuPd<sup>111</sup>. Most recently, they developed the synthesis of core-shell Ni/FePt nanomaterials and demonstrated the importance of Ni surface on the construction of alloy shell.<sup>122</sup> The avoidance of surface oxidation of the preformed zero-valence Ni seeds was crucial to successfully deposit a uniform FePt layer. They claimed that when Ni was oxidized to NiO, the large lattice mismatch between the oxide

medium and the preparation of Pd@Pt–Ni octahedra. The Pd octahedra were synthesized by reducing  $\text{Na}_2\text{PdCl}_4$  in a hydrophilic medium containing PVP, ethanol, and water. Due to the amphiphilic property of benzyl alcohol, the PVP-capped Pd octahedra could be collected by centrifugation and then redispersed in benzyl alcohol. The Pd@Pt–Ni core-shell octahedra were obtained by heating a mixture of Pd octahedra,  $\text{Pt}(\text{acac})_2$ ,  $\text{Ni}(\text{acac})_2$ ,  $\text{W}(\text{CO})_6$ , oleylamine, and oleic acid in benzyl alcohol at 200 °C for 40 min. TEM images of (b) PVP-capped Pd octahedral seeds with an edge length of 6 nm and (c) Pd@Pt–Ni octahedra with an edge length of 8 nm (together with a shell thickness of 1 nm). (Modified with permission from ref. 123. Copyright 2014, American Chemical Society.)

and Pt/FePt led the formation of separated FePt nanoparticles instead of alloy layer. After the Ni seeds were successfully protected from oxygen, FePt layer could be uniformly deposited. What is more, controlling the FePt nucleation and growth rate under a low level with the combination of oleic acid and oleylamine was also important to suppress the homogeneous nucleation of FePt. Burst nucleation of FePt happened and separated FePt nanoparticles formed in the absence of oleylamine. Their results exhibit the importance of the control of interfacial lattice mismatch and second step growth kinetics for constructing core-shell nanoparticles. In another case, octahedral core-shell Pd@Pt–Ni nanocrystals (Fig.13c) were fabricated through the appropriate introduction of a kind of amphiphilic molecules.<sup>123</sup> Shaped Pd seeds were first synthesized in hydrophilic environment and encapsulated by PVP (Fig.13b). After purification of the Pd seeds, amphiphilic benzyl alcohol was utilized to endow the compatibility between the hydrophilic seeds with the hydrophobic shell growth environment as shown in Fig.13a. If the second process was conducted in hydrophilic solvent containing water, Ni on the shell surface would be oxidized into  $\text{Ni}_x\text{O}_y$ ; irregular core-shell like nanoparticles instead of octahedral structure formed when benzyl alcohol was replaced by less hydrophilic solvent. High mixture free energy of mixing hydrophilic seeds with hydrophobic growth environment inhibits the nucleation and growth of shell metals on the preformed seeds. Introducing an appropriate amphiphilic solvent can effectively reduce the mixture free energy and facilitate the formation of core-shell nanostructures. When alloy nanoparticles are synthesized first and utilized as seeds, core-shell alloy/metal nanostructures can be formed. Murray et al. reported the strategy to construct core-shell  $\text{Pt}_3\text{Pb}/\text{Pt}$  with preformed  $\text{Pt}_3\text{Pb}$  seeds.<sup>124</sup> As discussed before, the reaction temperature of second step had a key impact on the shell

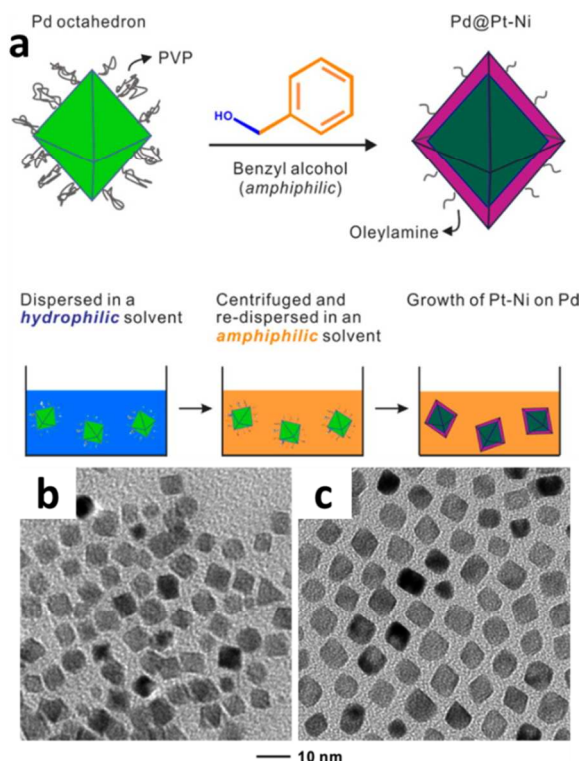


**Figure 13.** (a) Schematic illustration of a procedure used to transfer the Pd nanocrystals from a hydrophilic solvent to an amphiphilic reaction

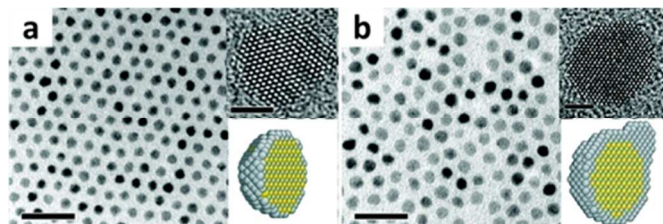


**Figure 14.** TEM images and (insets) HRTEM images of (a) Pt<sub>3</sub>Pb/Pt (layer growth) nanocrystals, and (b) Pt<sub>3</sub>Pb/Pt (intermediate growth) nanocrystals. Scale bars: 20 nm, (insets) 2 nm. (Modified with permission from ref. 124. Copyright 2012, American Chemical Society)

growth mode. Low temperature resulted in low reduction rate and led to layered growth of Pt shell as shown Fig.14a. However intermediate growth mode happened under higher temperature (Fig.14b). Later, the fabrication of core-shell AuCu/Pt with AuCu alloy seeds was reported.<sup>125</sup> The negligible lattice mismatch between AuCu and Pt facilitated the layered growth mode. And when alloy seeds are chosen to grow alloy shell, more complex core-shell alloy/alloy nanoparticles can form. The examples can be found in core-shell Pt<sub>3</sub>Ni/Pt<sub>3</sub>Pd and FePtM/FePt (M=Pd, Au) nanocrystals.<sup>126</sup> Through sequentially utilizing the seed-mediated method, core-shell nanoparticles with multilayered structures can be obtained. Generally, the inner core can enhance the stability during catalytic process and the interlayered metals can modify the structure of the outmost layered metals. Very recently, shaped Pd-Ni-Pt core-sandwich-shell nanoparticles were synthesized by Tsung's group through a layer-by-layer epitaxial overgrowth approach.<sup>127</sup> Cubic Pd seeds were fabricated for sequential loading of Ni and Pt layers in aqueous with CTAB as the colloidal stabilizer and hydrazine as the reductant. The final morphology of the sandwich nanoparticles were confined by the shape of the Pd seeds and the limited growth of {100} facets capped and stabilized by Br<sup>-</sup>. The thickness of Ni interlayer could be tuned through changing the amount of Ni precursor. It is obvious that this route is effective but needs multiple steps.

With the comparison to seed-mediated growth, one-pot core-reduction synthetic route for multimetallic core-shell nanostructures seems to be more convenient. However, the control of the nucleation and growth of multiple metals with different redox potentials for the formation of well-confined core-shell nanostructures rather than totally alloy or separated nanoparticles in just one step is more complicated and difficult. The strategy to fabricate trimetallic Au@PdPt core-shell NPs with a well-defined octahedral Au core and a dendritic PdPt alloy shell with no seeds or template was reported by Han's group.<sup>128</sup> The key point is to conduct the reaction under dual reducing agents, ascorbic acid and hydrazine, which provided powerful control of the nucleation and growth kinetics within an appropriate region. With only ascorbic acid, dendritic PdPt alloy nanoparticles were observed without Au although Au precursors possess a higher reduction potential both than Pd and Pt ones. When hydrazine was solely used as the reductant, only polyhedral Au nanoparticles formed without Pt or Pd. Due to the complication and difficulty of control over the entire nucleation and growth kinetics of multiple metals in one step, the examples on one-pot synthesis of multimetallic core-shell nanocrystals are still limited.

Besides to the colloidal chemistry methods, other routes such as under potential deposition,<sup>129, 130</sup> electrochemical dealloy,<sup>131</sup> and reaction driven approach<sup>132</sup> can also synthesize

core-shell nanocrystals but always combine with the discussed colloidal chemistry methods. In this review, detailed discussions on these methods are not focused.

### 3. Electrocatalytic property

To realize the commercialization of FCs based on noble metal nanomaterials, improving the electrocatalytic performance and minimizing the usage of precious metals are the long-term tasks. Nowadays the goal has been approached through the development of the synthesis of alloy nanoparticles with well-defined shapes.<sup>9, 13, 109, 118</sup> Their improved catalytic performance can be explained mainly by three effects: ligand effect, geometric effect and ensemble effect.<sup>4</sup> Ligand effect appears when guest metals are introduced and the electronic charge transfer between different atoms happens. In this case, the d-band center of nanoparticles shifts and the adsorption energies of reactants, intermediates and products on metal surface vary, leading to the modification of catalytic performance. Add Nørskov and co-workers established databases of d-band center of various bimetallic alloys and correlated the d-band center to chemisorption of molecules on the catalysts surface and consequent catalytic performance.<sup>7, 133, 134</sup> Then Umit B. Demirci utilized the databases to discuss the catalytic behaviors of alloy nanoparticles towards methanol, ethanol and formic acid electro-oxidations and also suggested the probable combinations of different metals with expected performance.<sup>135</sup> The databases of d-band center derive from the theoretical calculations, recently, a 'volcano-type' relationship between the experimentally obtained d-band center of different bimetallic nanoparticles and the dependent oxygen reduction reaction (ORR) activity on cathode was contributed.<sup>8</sup> The results showed that a suitable d-band center position which could well balance the adsorption of reactive intermediates and surface coverage of blocking species was highly expected to obtain optimal ORR kinetics. Geometric effect arises when atomic arrangement changes from initial pattern and results in strain on catalysts surface. The effect influences the distance of atoms and resulted overlapping level of d-orbitals, leading to the shift of d-band center. The experimental supports were reported by Strasser's group.<sup>4</sup> Ensemble effect exists if new geometries of the coordination of the adsorbates and reaction complexes on catalysts surface are provided through the introduction of guest metals.<sup>5</sup> This effect of different Pd atomic patterns in Au substrate on the electrocatalysis was already studied.<sup>6</sup> It showed that the smallest critical ensemble for the adsorption and oxidation of CO was Pd monomers, while at least Pd dimers are needed for the adsorption of H<sub>2</sub>. Therefore the formation of alloy structures promises the modification of their catalytic performance through any of the above-mentioned effects. In practical electrocatalytic processes, the combination of two or even all the three effects always coexists and simultaneously determines the resulted catalytic performance.

In this section, we highlight the recent developments of the modification and improvement of electrocatalytic performance in alloy noble metal nanocrystals with complex structures. For

core-shell nanoparticles, the approaches to modify the catalytic behaviors through engineering their lattice strain are emphasized. In nanoframes/nanocages, ultrathin nanocrystals, the point is put on that the high surface area can effectively maximize the discussed three effects to a greatest extent. The improved performance from the active sites including high-density low-coordinated atoms in steps, edges and kinks in nanocrystals with concave/convex and branched structures is chosen to be discussed.

### 3.1 Tunable lattice strain

Lattice strain in nanocrystals can be constructed due to several reasons including finite size,<sup>136, 137</sup> lattice mismatch,<sup>4, 138, 139</sup> local deformation, phase transformation<sup>140</sup> and element migration.<sup>141, 142</sup> The lattice strain indirectly influences the electronic structures of the nanocatalysts which actually modify the corresponding catalytic performance. As for core-shell nanostructures, the strain forms mainly due to the lattice mismatch between the core and shell components. Both compressive and tensile stress can form on the shell surface. A smaller lattice constant in core than that in shell tends to cause compressive strain in the nanoparticles surface. When compressive stress is identified by a decrease in the lattice constant of a nanoparticle, the bond length among atoms shortens. And tensile stress leads to the opposed result of elongation of the bond length. The variety of the bond length directly changes the distance between atoms and thus influences the overlapping level of the atoms' d-orbitals. The overlapping is decreased when the atoms are pulled faster under tensile strain. Then electrons with higher energy are required to complement the d occupancy, causing the d-band center upshift.<sup>143</sup> Oppositely, the d-band center downshifts under compressive strain. As mentioned, the shift of d-band center influences the chemisorption of species on catalysts surface and thus modifies the catalytic performance. The correlation between lattice strain and ORR activity in dealloyed Pt-Cu nanoparticles with a Pt-rich shell has already been established.<sup>4</sup> Lattice strain in the Pt-rich shell was tuned through changing the Pt-Cu composition of the core beneath. Based on the isolated strain effect, their results showed that different Pt-Cu compositions led to the different levels of compressive stress, leading to the distinct modifications of the electrocatalytic performance. In one word, the lattice strain can indirectly but effectively tune the catalytic performance. Nowadays the tunability has been extensively studied with the development of the synthesis of well-defined core-shell nanocrystals with complex structures. The overall lattice strain in the surface of a core-shell nanoparticle is always influenced by the core. The strain modification has been realized through controlling the composition, structure and thickness of the core (or interlayer). Based on the discussed multicomponent and multilayered core-shell nanostructures, we tend to emphasize the tunable lattice strain and the consequent variety in related electrocatalytic performance.

As demonstrated in some cases, {111} facets of noble metals are sometimes desired due to the relatively high activity and stability.<sup>9, 144</sup> Recently, multiply twinned icosahedral Ag seeds were utilized to grow uniform Pt shell enclosed by {111} facets for ORR.<sup>145</sup> However, the larger lattice constant of Ag tended to cause undesired tensile stress and consequent upshifted d-band center in the Pt shell. Then Pd was alloyed into the core to reduce the tensile stress and the AgPd@Pt/C showed higher activity than that of commercial Pt/C. The twinned structure might also create desired strain effect which was previously observed in icosahedral Pt<sub>3</sub>Ni and PtPd nanoparticles.<sup>146, 147</sup> For core-shell structures, chemically stable Au is always considered as a kind of promising core material to improve the stability of noble metal nanocrystals for the applications in electrochemical reactions. The well-established hindered place-exchange mechanism behind the enhancement of the durability has been demonstrated by many high-quality literatures.<sup>113, 148, 149</sup> In this case, the less favourable oxidation of Au under the shell can effectively hinder the migration of atomic oxygen from surface to subsurface sites, hence suppressing the dissolution of surface active species and improving the stability. Besides this mechanism, Au atoms in core can also significantly enhance the stability through modifying the electronic structure of shell active metal to low-lying d-band states. Although it is an effective route to improve the durability with the construction of Au core, the tensile stress in the shell coming from the lattice mismatch between Au and surface active metal (mostly Pt) is undesired. As mentioned above, alloying second metal with smaller lattice constant into the core can effectively reduce the tensile stress which was also demonstrated in the typical example of AuCu@Pt.<sup>125</sup> This material showed both high reaction active and excellent stability. The effective reduction of tensile stress through alloying second metal with smaller lattice constant into the core was also demonstrated in AuCu@Pt.<sup>125</sup> According to Vegard's law, the lattice constant would change when a second metal is introduced.<sup>138</sup> Thus constructing alloy core with different metals can tune the lattice constant of the core and hence vary the extent of strain in the shell surface.

The lattice strain effect of electrochemically dealloyed core-shell nanoparticles with Pt-rich shell on ORR performance has already been observed.<sup>4, 150</sup> In 2012, a significant study on the ORR performance of three typical dealloyed (D) Pt<sub>x</sub>Ni<sub>1-x</sub> core-shell nanoparticles was contributed by Strasser's group.<sup>151</sup> Through atomic scale characterization, the nanocrystals dealloyed from PtNi, PtNi<sub>3</sub> and PtNi<sub>5</sub> nanoparticles were demonstrated to possess different near-surface structures (Fig.15) which led to the variety in lattice strain and consequent ORR performance. The D-PtNi<sub>3</sub> showed the highest performance. At the comparable depth in the nanoparticles, the Ni component in D-PtNi<sub>3</sub> was higher than that in D-PtNi because more Ni existed in the inner shell of D-PtNi<sub>3</sub>. Thus more compressive strain was formed on D-PtNi<sub>3</sub> surface, leading to higher activity. As for D-PtNi<sub>5</sub>, although higher compressive strain was expected to form due to the thinner Pt shell, the lower Ni

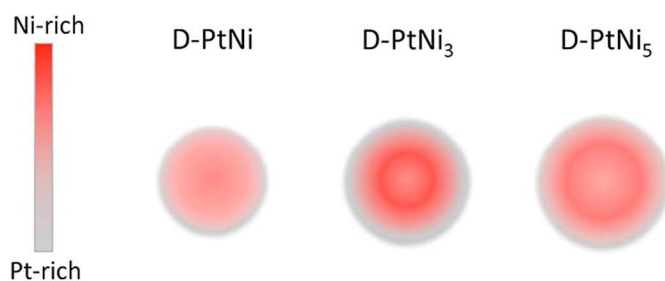


**Figure 15.** Structural model of distinctly different compositional core-shell fine structures of dealloyed  $Pt_xNi_{1-x}$  catalysts. (Adapted with permission from ref.151. Copyright 2012, American Chemical Society.)

component in the inner shell compared with D-PtNi<sub>3</sub> offset the effect. Together with the undesired rough surface, the activity of D-PtNi<sub>5</sub> was also lower. The study demonstrates the ORR activity of dealloyed core-shell nanoparticles mainly depends on the level of the lattice strain in the Pt-rich shell. Therefore controlling the composition of initial nanoparticles can modify the catalytic performance through the variable lattice strain.

Tsung's group synthesized cubic multilayered Pd-Ni-Pt sandwich nanoparticles with different thicknesses of Ni layer as a model platform to investigate the lattice strain effect on methanol and formic acid electro-oxidations.<sup>127</sup> The performance of sandwich nanoparticles with 2.5-nm and 4.1-nm Ni layers was compared to study the thickness-related catalytic activity. Their results showed that nanoparticles with thinner Ni layer were more active in all of the operated reactions. They claimed that thinner Ni layer under the Pt shell led to more strain effect with a consequent higher catalytic performance. Although they didn't give the mechanism behind the variety of the strain, it provides a guideline to design multilayered catalysts with improved performance.

More recently, a systemic study on the relationship between surface strain and ORR performance was established by Sun's group.<sup>152</sup> They combined several approaches to construct a series of samples: FePt/Pt core-shell nanoparticles with face centered cubic core (fcc-FePt/Pt), FePt/Pt core-shell nanoparticles with intermetallic face centered tetragonal (fct-FePt/Pt) transformed from fcc-FePt/Pt; after alloying the cores with Cu, they were denoted as fcc-FeCuPt/Pt and fct-FeCuPt/Pt. Through DFT calculation, the lattice strain and  $\Delta E_O$  (the exceeded value of Pt-O binding energy than that on the Pt (111) facets) values of the studied samples were obtained.  $\Delta E_O$  is an effective descriptor to assess the adsorption/desorption of oxygenated species on catalysts surface. The ORR activity of fct-FePt/Pt was higher than that of fcc-FePt/Pt due to its closer  $\Delta E_O$  value to 0.2eV. The lower  $\Delta E_O$  value came from the relieve of the overcompression after the structure transformation from fcc to fct. When the cores were alloyed with Cu, the performance was further improved resulted from the more relieve effect (Fig.16a). The fct-FeCuPt/Pt possessed the highest activity and durability as shown in Fig.16b-d. The durability

might be partly assigned to the intermetallic core structure which was also observed in  $Pt_3Fe_2$ <sup>153</sup> and platinum-cobalt<sup>154</sup> intermetallic core-shell nanocatalysts. Their work demonstrates that the surface strain can be tuned through changing the crystalline phase of core. It should be noticed that both the sizes and compositions of the nanoparticles are well maintained after structure transformations of the cores. And the strain effect is isolated due to the 3 atomic Pt layers which inhibits the ligand effect. Therefore the comparison is highly reliable.

To meet the requirement for developing new catalysts with improved performance, the modification of the lattice strain in nanoparticles has been demonstrated as an effective approach. While the quantitative characterization of lattice strain of nanoparticles with different structures and compositions is highly required and remains a challenge.<sup>155</sup>

### 3.2 High specific surface area

To develop innovative nanomaterials with improved catalytic

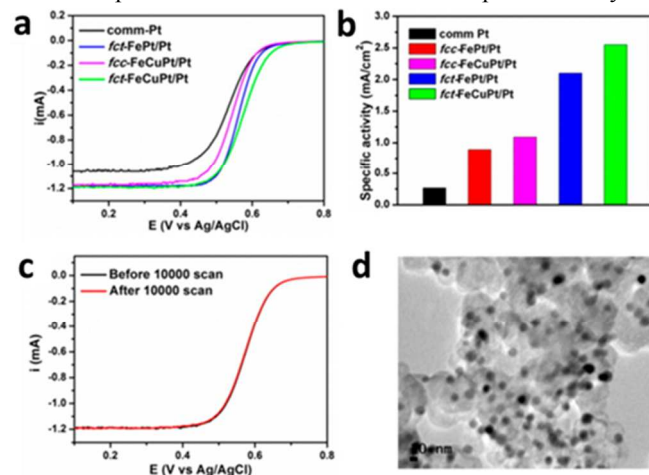


**Figure 16.** (a) ORR polarization curves of Pt, fct-FePt/Pt, fcc-FeCuPt/Pt, and fct-FeCuPt/nanoparticles. (b) The specific activities of the nanoparticle catalysts at 0.531 V ( $E_{1/2}$  of the commercial Pt catalyst). (c) ORR polarization curves of the fct-FeCuPt/Pt nanoparticles before and after 10 000 potential scans between 0.4 and 0.7 V. (d) TEM image of the fct-FeCuPt/Pt nanoparticles after 10 000 potential scans. (Adapted with permission from ref.152. Copyright 2014, American Chemical Society.)

performance, nanoparticles with specific geometric shapes and related high specific surface area have been immensely studied in recent years. Noble metal nanocrystals with unique structures such as nanoframes/nanocages and ultrathin structures usually exhibit the desirable feature which promises them as effective catalysts. It is obvious that optimizing at least one of the discussed three kinds of effects in deed endow a promising catalyst with intrinsic merits. On the other hand, one undoubted point is that constructing high surface area can effectively expose the optimized merits and further improve the catalytic performance. At the same time, the utilization of noble metal is promised to be increased which is of great significance for the

commercialization of noble metal-based nanomaterials. Based on this perspective, we tend to emphasize the recent achievements of excellent electrocatalytic performance in these structures especially those with the combination of modified effects and the successful extension of specific surface.

Nanoframes or nanocages are a kind of typical open nanostructures constructed by three-dimensional edges. The open structures can provide the opportunity for reactive molecules to be adsorbed on both the exterior and interior surfaces. Thus the special structures are reasonably able to provide high specific surface area which is of great significance for catalysts. And they usually exhibit desired durability during the catalytic process. In a typical example, the ORR catalytic activities of a series of octahedral and cubic Pd-Pt nanoparticles with different hollow levels were systematically studied.<sup>39</sup> All the nanoparticles were confirmed to produce a low yield of  $\text{H}_2\text{O}_2$  which demonstrated a high selectivity for desired four-electron reduction of oxygen during the ORR process. While the hollow octahedral and cubic Pt-Pd nanocages with porous walls owned higher ORR activities compared with the counterparts with lower hollow levels. The enhanced properties were ascribed to their smooth surface and more open structures which resulted in high ECSAs. The activity of octahedral nanocages was the highest due to the large exposure of more active Pt-Pd (111) facets. Lou's group reported a class of cubic Cu-rich intermetallic  $\text{PtCu}_3$  nanocages with high methanol electro-oxidation activity.<sup>47</sup> After electrochemical dealloying

Tafel plots of  $\text{Pt}_3\text{Ni}$  frames before and after 10,000 potential cycles between 0.6 and 1.0 V. (d and e) Bright-field STEM image (d) and dark-field STEM image (e) of  $\text{Pt}_3\text{Ni}$  nanoframes/C after cycles. (Modified with the permission from ref. 13. Copyright 2014, American Association for the Advancement of Science.)

process, the ratio of Pt/Cu was transformed from 1: 3 to 3:1 due to the dissolution of Cu, while the special structure was well maintained. Compared with  $\text{PtCu}_x$  solid nanoparticles ( $x \approx 9$ ), the dealloyed Pt/Cu nanocages were tested to show a higher ECSAs of  $35.7 \text{ m}^2 \text{ g}^{-1}$  and 3 times higher oxidation current density. And the value of  $I_f/I_b$  was much higher than that of commercial Pt/C which exhibited a more effective methanol oxidation and low production of poisoning species. The obviously improved catalytic activity of  $\text{PtCu}_3$  nanocages after dealloying should be first assigned to the rearrangement of Cu and Pt atoms which modified the electronic structure of the dealloyed surface to an optimal level for the methanol electro-oxidation. And when the surface with tuned electronic structure was extended to a high area because of the unique morphology, expectedly improved catalytic property appeared comparing with  $\text{PtCu}_x$  solid nanoparticles. Most recently, a dramatic improvement of ORR performance was realized by Yang's group through fabricating highly crystalline  $\text{Pt}_3\text{Ni}$  nanoframes.<sup>13</sup> Although at least two Pt monolayers skin rather than one Pt monolayer were confirmed to form on the Pt-skin-terminated (111)-like surface, the author claimed the existence of altered electronic structure with downshifted d-band center of Pt atoms on the surface. In this case, the bonding energy of Pt atoms with oxygenate species decreased, leading to high ORR kinetics. And the strain effect was demonstrated at an optimal level to facilitate the ORR process. The ligand and geometric effects together modified the electronic structure of surface metals which intrinsically improve the catalytic activity of the nanoframes. What's more, both the effects were maximized through the open nanoframe structure with the three-dimensional accessibility for molecules. The nanoframes showed surprising 22 times higher ORR mass activity compared with commercial Pt/C and negligible activity loss (Fig.17c) and morphology change after 10,000 cycles as illustrated in Fig.17d,e. Due to the capillary forces in the nanoframes, ionic liquid with the ability of dissolving  $\text{O}_2$  was readily entrapped into the nanoparticles and the ORR activity was further improved to a factor of 36 enhancement in mass activity (Fig.17b) and a factor of 22 enhancement in specific activity relative to Pt/C catalysts. (Fig.17a). Their work demonstrates that the nanoframe structures can provide not only high specific surface area and durability but also the possibility of trapping functional liquids which promise them further enhanced catalytic performance.

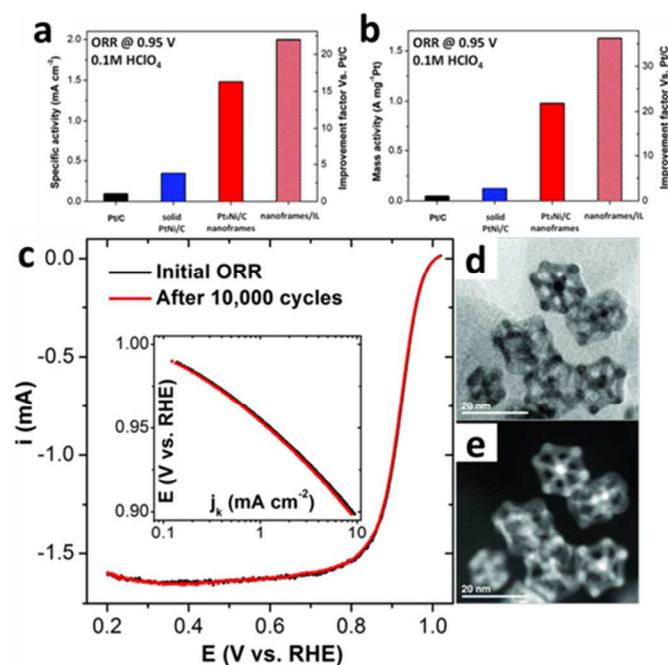


**Figure 17.** Specific activities (a) and mass activities (b) measured at 0.95 V, and improvement factors versus Pt/C catalysts. Because of the high intrinsic activity of the  $\text{Pt}_3\text{Ni}$  nanoframes, the ORR activity values are given at 0.95 V in order to avoid the extensive error margin at 0.9 V introduced by the close proximity of current values to the diffusion-limited current. IL, ionic liquid. Electrochemical durability of  $\text{Pt}_3\text{Ni}$  nanoframes. (c) ORR polarization curves and (inset) corresponding

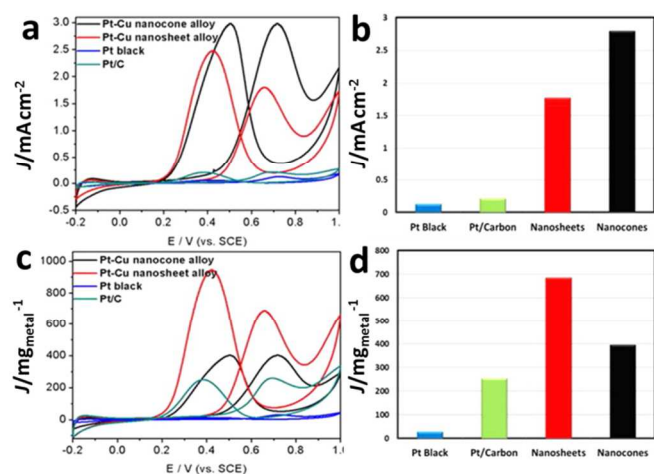


**Figure 18.** Comparison of electrocatalytic properties of the Pt–Cu nanocone alloy, Pt–Cu nanosheet alloy, Pt black, and Pt/C catalyst: (a) specific activity, (c) mass activity for these catalysts; (b, d) graphical comparison of specific and mass activities of all catalysts, respectively. Specific and mass activities are given as kinetic current densities ( $J$ ) normalized with reference to the ECSA and loading amount of metal, respectively. The ethanol oxidation was recorded in 0.5 M  $\text{H}_2\text{SO}_4$  + 0.1 M  $\text{CH}_3\text{CH}_2\text{OH}$  solution at a scan rate of 50 mV/s. (Modified with the permission from ref. 109. Copyright 2013, American Chemical Society.)

For noble metal nanomaterials with ultrathin structures, the atoms in the bulk are highly exposed on the surface. In this case, expectedly high mass activity usually arises, leading to the effective utilization of precious metals. Our group observed desirably high ethanol electro-oxidation activities of ultrathin Pt–Cu alloy nanosheets with 4-atom thickness and nanocones rolling from the nanosheets.<sup>109</sup> The specific active factors of the ultrathin nanosheets and nanocones were 22 times and 14 times that of Pt black as shown in Fig.18a, b. Besides the significant ligand effect resulting from the interaction of electrons in Cu and Pt atoms, we proposed that the enhanced catalytic performance further resulted from the specific geometric shapes of the ultrathin structures. And the 4-atom thickness of the ultrathin nanosheets led to a high exposure of the atoms in the bulk to the surface, thus resulting in 19 times higher mass activity than that of Pt black (Fig.18c, d). Our results demonstrate that construction of ultrathin nanostructures is an effective approach to gain the improvement of catalytic performance especially high mass activity. Another case of enhanced mass activity was observed in excavated rhombic dodecahedral  $\text{PtCu}_3$  alloy nanostructures constructed with ultrathin nanosheets solely exposing high-energy  $\{110\}$  facets.<sup>12</sup> With comparison to the nanoparticles enclosed by a mixture of  $\{111\}$  and  $\{110\}$  facets, the  $\{110\}$  facets were demonstrated to possess higher activity towards formic acid electro-oxidation and better tolerance of CO. The thickness of the nanosheets was 2 nm, thus Pt atoms were effectively exposed on the catalysts surface and consequent high mass activity of 2.63 times that of commercial Pt black was observed.

What's more, the EDR structure showed excellent stability during the electrochemical reaction process. Besides the promising tolerance of CO mainly resulting from the intrinsic electronic structure of the alloy nanocrystals, the unique morphology with a 3-dimensional broad spatial distribution of active sites which endowed the structure with decreased trend to aggregate also made a contribution to the stability.

As catalytic reactions proceed on nanoparticles surface in heterogeneous catalysis, the design of highly active surface is of great significance to obtain expected catalytic performance. According to the discussed cases, it is clear that whenever the high active surfaces are already constructed, the above-mentioned structures with large surface area can further extend the desirable surfaces. Thus much higher catalytic activity can be observed. Especially for ultrathin structures, enhanced mass activity and consequent effective utilization of precious metals are always obtained due to the large exposure of bulk atoms in the bulk to their surfaces.

### 3.3 High active sites

Considerable electrocatalytic performance of noble metal nanocrystals enclosed by high-index facets has already been extensively observed and investigated.<sup>65, 156, 157</sup> The promising properties are ascribed to the existence of high density of low-coordinated atoms in steps, edges and kinks which are catalytically active sites on their surfaces. A significant work on the synthesis of tetrahedral Pt nanocrystals enclosed by 24 high-index facets such as  $\{730\}$ ,  $\{210\}$ , and/or  $\{520\}$  surfaces was contributed by Wang and Sun et al.<sup>65</sup> The nanoparticles were demonstrated to possess dramatically enhanced activity in formic acid and ethanol electro-oxidations due to the exposure of high density of active atomic steps and dangling bonds. In this subsection, desirable electrocatalytic performance arising from these high active sites mainly on the surface of concave, convex, and other special shapes such as branched structures are highlighted.

AuPd alloy nanoparticles have exhibited higher catalytic activity towards ethanol electro-oxidation in alkaline media than Pt-based and Pd nanoparticles. To develop this class of catalysts, AuPd nanoparticles with high-index facets providing high density of active sites on their surfaces have been more extensively studied. Trisuboctahedral Au–Pd alloy nanocrystals enclosed by high-index  $\{221\}$  facets and hexoctahedral ones enclosed by  $\{541\}$  and  $\{421\}$  facets were confirmed to show higher ethanol electro-oxidation activities than that of the counterparts with low-index facets and commercial Pd black.<sup>73</sup> Xu's group fabricated branched concave AuPd nanocrystals and observed superior catalytic activity towards ethanol oxidation.<sup>62</sup> Through detailed TEM measurements, the side facets of every single branch were identified as  $\{411\}$  facets, exposing step atoms which created altered (111) and (100) sub-facets. The nanoparticles showed a specific activity of 7-8 times higher than that of spherical AuPd nanoparticles. The enhanced performance arose due to the high density of step atoms on the high-index  $\{411\}$  facets and synergic action of Au and Pd.

Based on the unique branched structure with high surface area, the nanoparticles desirably exhibited even 9 times higher mass activity with the comparison to commercial Pt/C.

Alloying early transition metals (Fe, Co, Ni...) with precious metals is an effective approach to improve the catalytic property and reduce the cost of noble-metal-based nanomaterials. Yan's group co-introduced Pd and Cu to synthesize trimetallic concave Pt-Pd-Cu nanoparticles and gained enhanced methanol electro-oxidation activity.<sup>70</sup> For the same reaction, Li's group further improved the catalytic performance with both high specific activity and tolerance to CO poisoning through the successful construction of a series of Pt/Ni concave nanoparticles.<sup>67</sup> The nanocrystals surface exposed segregated Pt atomic steps which could effectively oxidize CO intermediates. Then they reported Pt/Cu hexapod concave nanocrystals with high-index {112} facets which showed 2.5 times higher activity of methanol electro-oxidation than that of commercial Pt black.<sup>60</sup> The introduced transition metals could tune the electronic structures of host metals and then modify the adsorption energy of molecules on catalysts surface. When the adsorption energy of CO intermediates was decreased, the electro-oxidation performance was enhanced because of more freshly active sites on catalysts surface. Recently, Pt/Ni nanoparticles with different structures have been demonstrated as promising catalysts for ORR.<sup>9</sup> However the cases of Pt/Ni nanocrystals with high-index facets for this application are still limited. Most recently, Zhang and Sun et al. synthesized concave-cubic and hexoctahedral Pt-Ni alloys with a series of {hkl} and {hk0} high-index facets.<sup>75</sup> Hexoctahedral Pt-Ni nanoparticles showed 5 times higher specific activity towards ORR compared with Pt/C due to their high-density atomic steps and kinks and the electronic effect of the formed alloy. And both the concave-cubic and hexoctahedral nanoparticles exhibited enhanced activities of methanol and formic acid electro-oxidations. However, their mass activities were lower than that of Pt/C owing to the relatively large particle sizes. Thus in the future, more efforts on developing nanoparticles with both small sizes and high-index facets should be made to meet the requirement for improving their catalytic performance.

#### 4. Conclusion and perspective

Under the requirement for developing sustainable and environmentally friendly technologies on chemical transformations and energy conversion, tremendous efforts have been devoted to fabricate noble metal nanocrystals used as electrode materials in FCs. Nowadays, various multicomponent noble metal nanocrystals with the architectures including nanoframes/nanocages, branched structures, concave/convex structures, ultrathin structures and core-shell structures have been controllably synthesized through well-designed strategies. According to individual typical structures, the special synthetic routes are delivered and the key factors and mechanisms behind are discussed and compared. Through the construction of these noble metal alloy complex nanostructures, the related

electrocatalytic performance has indeed been greatly improved and the usage of precious metals has been effectively minimized. Based on the organization of synthesis sections, the catalytic properties from distinct complex structures are exhibited.

Besides the satisfactory achievements in this field, there still exist many significant challenges. Among the various shape controllers, surfactants or capping agents have been demonstrated as one of the most effective factors to control the complex structures of noble metal nanomaterials. While the mechanisms behind are poorly understood due to the insufficient information on the understanding of the molecule-level interactions between the surfactants and the growing facets at different growth stages. To solve this issue, the recent developments of theoretical calculations on the interaction modes and the surface energy of facets with capping agents should be promised to gain predicts and guidelines. More importantly, the lack of high-quantity production methods of noble metal nanocrystals with well-confined structures greatly limits the commercialization of such materials. As for the electrochemical catalysis, although dramatically improved performance has been obtained through constructing catalysts with specific structures, most of the evaluations are limited in laboratory. To further predict the possibility of the commercialization of noble metal nanomaterials, the tests in actual fuel cells systems should be well established. Furthermore, the surface of noble metal nanomaterials with well-defined structures is usually tightly bonded by capping agents which will have a negative effect on the catalytic performance. Thus appropriate methods should be developed to remove the capping agents, coupled with negligible influence on the morphology of the nanocrystals. One of the biggest challenges is to deeply understand the mechanisms behind the catalysis process. On one hand, many effects can simultaneously determine the catalytic performance of a catalyst, making it difficult to distinguish how the individual effect influences the final catalysis. When the study is mainly based on experiment data, the target effect should be isolated from other effects. On the other hand, the surface structures of noble metal nanoparticles are usually changed during electrochemical reactions. In many cases, the phenomenon of metal atoms dissolution, element segregation or surface reconstruction can be observed. The technologies on in situ studies which make a contribution to trace the evolution under reaction conditions should obtain more attentions to gain insights in this respect. Overall, the controllable synthetic methods are expected to provide effective study models to investigate the related properties. The fully understood mechanisms behind the properties in turn guide the design of promising materials. The final goal is to realize the large-scale production of noble metal materials with both improved performance and low cost.

## Acknowledgements

This work was supported by NSFC (21431003, 91127040, 21221062), and the State Key Project of Fundamental Research for Nanoscience and Nanotechnology (2011CB932402). Xun Wang acknowledges Collaborative Innovation Center of Chemical Science and Engineering (Tianjin).

## References

- 1 W. Yu, M. D. Porosoff and J. G. Chen, *Chem. Rev.*, 2012, **112**, 5780-5817.
- 2 M. K. Debe, *Nature*, 2012, **486**, 43-51.
- 3 N. Jung, D. Y. Chung, J. Ryu, S. J. Yoo and Y.-E. Sung, *Nano Today*, 2014, **9**, 433-456.
- 4 P. Strasser, S. Koh, T. Anniyev, J. Greeley, K. More, C. Yu, Z. Liu, S. Kaya, D. Nordlund and H. Ogasawara, *Nat. Chem.*, 2010, **2**, 454-460.
- 5 M. Chen, D. Kumar, C.-W. Yi and D. W. Goodman, *Science*, 2005, **310**, 291-293.
- 6 F. Maroun, F. Ozanam, O. Magnussen and R. Behm, *Science*, 2001, **293**, 1811-1814.
- 7 A. Ruban, B. Hammer, P. Stoltze, H. L. Skriver and J. K. Nørskov, *J. Mol. Catal. A*, 1997, **115**, 421-429.
- 8 V. R. Stamenkovic, B. S. Mun, M. Arenz, K. J. Mayrhofer, C. A. Lucas, G. Wang, P. N. Ross and N. M. Markovic, *Nat. Mater.*, 2007, **6**, 241-247.
- 9 V. R. Stamenkovic, B. Fowler, B. S. Mun, G. Wang, P. N. Ross, C. A. Lucas and N. M. Marković, *Science*, 2007, **315**, 493-497.
- 10 J. Zhang, H. Yang, J. Fang and S. Zou, *Nano Lett.*, 2010, **10**, 638-644.
- 11 A.-X. Yin, X.-Q. Min, Y.-W. Zhang and C.-H. Yan, *J. Am. Chem. Soc.*, 2011, **133**, 3816-3819.
- 12 Y. Jia, Y. Jiang, J. Zhang, L. Zhang, Q. Chen, Z. Xie and L. Zheng, *J. Am. Chem. Soc.*, 2014, **136**, 3748-3751.
- 13 C. Chen, Y. Kang, Z. Huo, Z. Zhu, W. Huang, H. L. Xin, J. D. Snyder, D. Li, J. A. Herron, M. Mavrikakis, M. Chi, K. L. More, Y. Li, N. M. Markovic, G. A. Somorjai, P. Yang and V. R. Stamenkovic, *Science*, 2014, **343**, 1339-1343.
- 14 Y. Yin and A. P. Alivisatos, *Nature*, 2005, **437**, 664-670.
- 15 Y. Xia, Y. Xiong, B. Lim and S. E. Skrabalak, *Angew. Chem. Int. Ed.*, 2009, **48**, 60-103.
- 16 X. Hong, C. Tan, J. Chen, Z. Xu and H. Zhang, *Nano Res.*, 2014, 40-55.
- 17 J. Gu, Y.-W. Zhang and F. F. Tao, *Chem. Soc. Rev.*, 2012, **41**, 8050-8065.
- 18 S. Guo and E. Wang, *Nano Today*, 2011, **6**, 240-264.
- 19 H. You, S. Yang, B. Ding and H. Yang, *Chem. Soc. Rev.*, 2013, **42**, 2880-2904.
- 20 J. Zeng, J. Huang, W. Lu, X. Wang, B. Wang, S. Zhang and J. Hou, *Adv. Mater.*, 2007, **19**, 2172-2176.
- 21 X. Yu, D. Wang, Q. Peng and Y. Li, *Chem. Commun.*, 2011, **47**, 8094-8096.
- 22 H. Liu, J. Qu, Y. Chen, J. Li, F. Ye, J. Y. Lee and J. Yang, *J. Am. Chem. Soc.*, 2012, **134**, 11602-11610.
- 23 Y. Song, R. M. Garcia, R. M. Dorin, H. Wang, Y. Qiu and J. A. Shelnett, *Angew. Chem. Int. Ed.*, 2006, **45**, 8126-8130.
- 24 J. Zeng, Q. Zhang, J. Chen and Y. Xia, *Nano Lett.*, 2009, **10**, 30-35.
- 25 M. McEachran, D. Keogh, B. Pietrobon, N. Cathcart, I. Gourevich, N. Coombs and V. Kitaev, *J. Am. Chem. Soc.*, 2011, **133**, 8066-8069.
- 26 S. E. Skrabalak, J. Chen, Y. Sun, X. Lu, L. Au, C. M. Cobley and Y. Xia, *Acc. Chem. Res.*, 2008, **41**, 1587-1595.
- 27 H.-J. Jang, S. Hong and S. Park, *J. Mater. Chem.*, 2012, **22**, 19792-19797.
- 28 K. M. Yeo, S. Choi, R. M. Anisur, J. Kim and I. S. Lee, *Angew. Chem. Int. Ed.*, 2011, **50**, 745-748.
- 29 L. Au, Y. Chen, F. Zhou, P. C. Camargo, B. Lim, Z.-Y. Li, D. Ginger and Y. Xia, *Nano Res.*, 2008, **1**, 441-449.
- 30 S. Xie, N. Lu, Z. Xie, J. Wang, M. J. Kim and Y. Xia, *Angew. Chem. Int. Ed.*, 2012, **51**, 10266-10270.
- 31 H. Wu, P. Wang, H. He and Y. Jin, *Nano Res.*, 2012, **5**, 135-144.
- 32 Y. Xiong, B. Wiley, J. Chen, Z. Y. Li, Y. Yin and Y. Xia, *Angew. Chem. Int. Ed.*, 2005, **44**, 7913-7917.
- 33 L. Gan, C. Cui, M. Heggen, F. Dionigi, S. Rudi and P. Strasser, *Science*, 2014, **346**, 1502-1506.
- 34 Y. Wang, Y. Chen, C. Nan, L. Li, D. Wang, Q. Peng and Y. Li, *Nano Res.*, 2014, 140-155.
- 35 Y. Wu, D. Wang, G. Zhou, R. Yu, C. Chen and Y. Li, *J. Am. Chem. Soc.*, 2014, **136**, 11594-11597.
- 36 X. Xia, Y. Wang, A. Ruditskiy and Y. Xia, *Adv. Mater.*, 2013, **25**, 6313-6333.
- 37 M. A. Mahmoud and M. A. El-Sayed, *Langmuir*, 2012, **28**, 4051-4059.
- 38 H. Zhang, M. Jin, H. Liu, J. Wang, M. J. Kim, D. Yang, Z. Xie, J. Liu and Y. Xia, *ACS Nano*, 2011, **5**, 8212-8222.
- 39 J. W. Hong, S. W. Kang, B.-S. Choi, D. Kim, S. B. Lee and S. W. Han, *ACS Nano*, 2012, **6**, 2410-2419.
- 40 C.-L. Lee, K.-L. Huang, Y.-L. Tsai and Y.-J. Chao, *Electrochem. Commun.*, 2013, **34**, 282-285.
- 41 M. Tsuji, M. Hamasaki, A. Yajima, M. Hattori, T. Tsuji and H. Kawazumi, *Mater. Lett.*, 2014, **121**, 113-117.
- 42 L. Tian, X. Zhong, W. Hu, B. Liu and Y. Li, *Nanoscale Res. Lett.*, 2014, **9**, 68-73.
- 43 X. Hong, D. Wang, S. Cai, H. Rong and Y. Li, *J. Am. Chem. Soc.*, 2012, **134**, 18165-18168.
- 44 X. Huang, H. Zhang, C. Guo, Z. Zhou and N. Zheng, *Angew. Chem. Int. Ed.*, 2009, **121**, 4902-4906.
- 45 Z. Zhang, Y. Yang, F. Nosheen, P. Wang, J. Zhang, J. Zhuang and X. Wang, *Small*, 2013, **9**, 3063-3069.
- 46 F. Nosheen, Z.-C. Zhang, J. Zhuang and X. Wang, *Nanoscale*, 2013, **5**, 3660-3663.
- 47 B. Y. Xia, H. B. Wu, X. Wang and X. W. Lou, *J. Am. Chem. Soc.*, 2012, **134**, 13934-13937.
- 48 L. Han, H. Liu, P. Cui, Z. Peng, S. Zhang and J. Yang, *Sci. Rep.*, 2014, **4**, 6414/6411-6414/6416.
- 49 D. Yoon, S. Park, J. Park, J. Kim, H. Baik, H. Yang and K. Lee, *Nanoscale*, 2014, **6**, 12397-12402.
- 50 B. Jeyadevan, J. L. Cuya, Y. Inoue, K. Shinoda, T. Ito, D. Mott, K. Higashimine, S. Maenosono, T. Matsumoto and H. Miyamura, *RSC Adv.*, 2014, **4**, 26667-26672.
- 51 C. H. Christopher C. Yec, Zeng, *J. Mater. Chem. A*, 2014, **2**, 4843-4851.
- 52 X. Wang, H. Fu, A. Peng, T. Zhai, Y. Ma, F. Yuan and J. Yao, *Adv. Mater.*, 2009, **21**, 1636-1640.

- 53 B. S. Choi, S. M. Kim, J. Gong, Y. W. Lee, S. W. Kang, H. S. Lee, J. Y. Park and S. W. Han, *Chem. Eur. J.*, 2014, **20**, 11669-11674.
- 54 E. Taylor, S. Chen, J. Tao, L. Wu, Y. Zhu and J. Chen, *ChemSusChem*, 2013, **6**, 1863-1867.
- 55 W. Wang, D. Wang, X. Liu, Q. Peng and Y. Li, *Chem. Commun.*, 2013, **49**, 2903-2905.
- 56 J.-N. Zheng, L.-L. He, F.-Y. Chen, A.-J. Wang, M.-W. Xue and J.-J. Feng, *J. Mater. Chem. A*, 2014, **2**, 12899-12906.
- 57 B. Lim, M. Jiang, P. H. C. Camargo, E. C. Cho, J. Tao, X. Lu, Y. Zhu and Y. Xia, *Science*, 2009, **324**, 1302-1305.
- 58 Z. Niu, D. Wang, R. Yu, Q. Peng and Y. Li, *Chem. Sci.*, 2012, **3**, 1925-1929.
- 59 Z.-Q. Zhang, J. Huang, L. Zhang, M. Sun, Y.-C. Wang, Y. Lin and J. Zeng, *Nanotechnology*, 2014, **25**, DOI:10.1088/0957-4484/1025/1043/435602.
- 60 X. Liu, W. Wang, H. Li, L. Li, G. Zhou, R. Yu, D. Wang and Y. Li, *Sci. Rep.*, 2013, **3**, 1404/1401-1404-1405.
- 61 R. He, Y.-C. Wang, X. Wang, Z. Wang, G. Liu, W. Zhou, L. Wen, Q. Li, X. Wang, X. Chen, J. Zeng and J. G. Hou, *Nat. Comm.*, 2014, **5**, 5327/5321-5327/5310.
- 62 L.-F. Zhang, S.-L. Zhong and A.-W. Xu, *Angew. Chem. Int. Ed.*, 2013, **52**, 645-649.
- 63 F. Nosheen, Z. Zhang, G. Xiang, B. Xu, Y. Yang, F. Saleem, X. Xu, J. Zhang and X. Wang, *Nano Res.*, 2014, DOI 10.1007/s12274-12014-10565-12271.
- 64 M. Gong, G. Fu, Y. Chen, Y. Tang and T. Lu, *ACS Appl. Mater. Interfaces*, 2014, **6**, 7301-7308.
- 65 N. Tian, Z.-Y. Zhou, S.-G. Sun, Y. Ding and Z. L. Wang, *Science*, 2007, **316**, 732-735.
- 66 M. J. Mulvihill, X. Y. Ling, J. Henzie and P. Yang, *J. Am. Chem. Soc.*, 2009, **132**, 268-274.
- 67 Y. Wu, D. Wang, Z. Niu, P. Chen, G. Zhou and Y. Li, *Angew. Chem. Int. Ed.*, 2012, **51**, 12524-12528.
- 68 H. Zhang, M. Jin, J. Wang, W. Li, P. H. C. Camargo, M. J. Kim, D. Yang, Z. Xie and Y. Xia, *J. Am. Chem. Soc.*, 2011, **133**, 6078-6089.
- 69 F. Zhan, T. Bian, W. Zhao, H. Zhang, M. Jin and D. Yang, *CrystEngComm*, 2014, **16**, 2411-2416.
- 70 A.-X. Yin, X.-Q. Min, W. Zhu, W.-C. Liu, Y.-W. Zhang and C.-H. Yan, *Chem. Eur. J.*, 2012, **18**, 777-782.
- 71 C. Wang, C. Lin, L. Zhang, Z. Quan, K. Sun, B. Zhao, F. Wang, N. Porter, Y. Wang and J. Fang, *Chem. Eur. J.*, 2014, **20**, 1753-1759.
- 72 J. Zhang, C. Hou, H. Huang, L. Zhang, Z. Jiang, G. Chen, Y. Jia, Q. Kuang, Z. Xie and L. Zheng, *Small*, 2013, **9**, 538-544.
- 73 Y. Qi, T. Bian, S.-I. Choi, Y. Jiang, C. Jin, M. Fu, H. Zhang and D. Yang, *Chem. Commun.*, 2014, **50**, 560-562.
- 74 L. Zhang, J. Zhang, Q. Kuang, S. Xie, Z. Jiang, Z. Xie and L. Zheng, *J. Am. Chem. Soc.*, 2011, **133**, 17114-17117.
- 75 X. Xu, X. Zhang, H. Sun, Y. Yang, X. Dai, J. Gao, X. Li, P. Zhang, H.-H. Wang, N.-F. Yu and S.-G. Sun, *Angew. Chem. Int. Ed.*, 2014, **53**, 12522-12527.
- 76 L. Zhang, W. Niu, Z. Li and G. Xu, *Chem. Commun.*, 2011, **47**, 10353-10355.
- 77 L. Zhang, W. Niu, J. Zhao, S. Zhu, Y. Yuan, T. Yuan, L. Hu and G. Xu, *Faraday Discuss.*, 2013, **164**, 175-188.
- 78 L. Zhang, W. Niu, W. Gao, L. Qi, J. Lai, J. Zhao and G. Xu, *ACS Nano*, 2014, **8**, 5953-5958.
- 79 D. Kim, Y. W. Lee, S. B. Lee and S. W. Han, *Angew. Chem. Int. Ed.*, 2012, **51**, 159-163.
- 80 L.-f. Zhang and C.-y. Zhang, *Nanoscale*, 2013, **5**, 6074-6080.
- 81 W. Wang, J. Zhang, S. Yang, B. Ding and X. Song, *ChemSusChem*, 2013, **6**, 1945-1951.
- 82 G.-R. Zhang, J. Wu and B.-Q. Xu, *J. Phys. Chem. C*, 2012, **116**, 20839-20847.
- 83 J. W. Hong, M. Kim, Y. Kim and S. W. Han, *Chem. Eur. J.*, 2012, **18**, 16626-16630.
- 84 H.-W. Liang, S. Liu, J.-Y. Gong, S.-B. Wang, L. Wang and S.-H. Yu, *Adv. Mater.*, 2009, **21**, 1850-1854.
- 85 L. Cademartiri and G. A. Ozin, *Adv. Mater.*, 2009, **21**, 1013-1020.
- 86 S. Hu and X. Wang, *Chem. Soc. Rev.*, 2013, **42**, 5577-5594.
- 87 S. Hu, H. Liu, P. Wang and X. Wang, *J. Am. Chem. Soc.*, 2013, **135**, 11115-11124.
- 88 P.-P. Wang, Y. Yang, J. Zhuang and X. Wang, *J. Am. Chem. Soc.*, 2013, **135**, 6834-6837.
- 89 Z. Fan, X. Huang, C. Tan and H. Zhang, *Chem. Sci.*, 2015, **6**, 95-111.
- 90 S. De, T. M. Higgins, P. E. Lyons, E. M. Doherty, P. N. Nirmalraj, W. J. Blau, J. J. Boland and J. N. Coleman, *ACS Nano*, 2009, **3**, 1767-1774.
- 91 X. Teng, M. Feygenon, Q. Wang, J. He, W. Du, A. I. Frenkel, W. Han and M. Aronson, *Nano Lett.*, 2009, **9**, 3177-3184.
- 92 X. Huang, S. Li, S. Wu, Y. Huang, F. Boey, C. L. Gan and H. Zhang, *Adv. Mater.*, 2012, **24**, 979-983.
- 93 M. Lu, M. K. Li, L. B. Kong, X. Y. Guo and H. L. Li, *Chem. Phys. Lett.*, 2003, **374**, 542-547.
- 94 T. A. Crowley, K. J. Ziegler, D. M. Lyons, D. Erts, H. Olin, M. A. Morris and J. D. Holmes, *Chem. Mater.*, 2003, **15**, 3518-3522.
- 95 C. Zhu, S. Guo and S. Dong, *Adv. Mater.*, 2012, **24**, 2326-2331.
- 96 C. Zhu, S. Guo and S. Dong, *J. Mater. Chem.*, 2012, **22**, 14851-14855.
- 97 X. Lu, M. S. Yavuz, H.-Y. Tuan, B. A. Korgel and Y. Xia, *J. Am. Chem. Soc.*, 2008, **130**, 8900-8901.
- 98 Z. Huo, C.-k. Tsung, W. Huang, X. Zhang and P. Yang, *Nano Lett.*, 2008, **8**, 2041-2044.
- 99 C. Wang, Y. Hou, J. Kim and S. Sun, *Angew. Chem. Int. Ed.*, 2007, **46**, 6333-6335.
- 100 S. Guo, S. Zhang, X. Sun and S. Sun, *J. Am. Chem. Soc.*, 2011, **133**, 15354-15357.
- 101 S. Guo, D. Li, H. Zhu, S. Zhang, N. M. Markovic, V. R. Stamenkovic and S. Sun, *Angew. Chem. Int. Ed.*, 2013, **52**, 3465-3468.
- 102 Z. Peng, H. You and H. Yang, *ACS Nano*, 2010, **4**, 1501-1510.
- 103 X. Hong, D. Wang, R. Yu, H. Yan, Y. Sun, L. He, Z. Niu, Q. Peng and Y. Li, *Chem. Commun.*, 2011, **47**, 5160-5162.
- 104 X. Yu, D. Wang, Q. Peng and Y. Li, *Chem. Eur. J.*, 2013, **19**, 233-239.
- 105 B. Y. Xia, H. B. Wu, Y. Yan, X. W. Lou and X. Wang, *J. Am. Chem. Soc.*, 2013, **135**, 9480-9485.
- 106 X. Huang, S. Tang, X. Mu, Y. Dai, G. Chen, Z. Zhou, F. Ruan, Z. Yang and N. Zheng, *Nat. Nanotech.*, 2011, **6**, 28-32.
- 107 X. Huang, S. Li, Y. Huang, S. Wu, X. Zhou, S. Li, C. L. Gan, F. Boey, C. A. Mirkin and H. Zhang, *Nat. Comm.*, 2011, **2**, 292.
- 108 H. Duan, N. Yan, R. Yu, C.-R. Chang, G. Zhou, H.-S. Hu, H. Rong, Z. Niu, J. Mao, H. Asakura, T. Tanaka, P. J. Dyson, J. Li and Y. Li, *Nat. Comm.*, 2014, **5**, 3093/3091-3093/3098.

- 109 F. Saleem, Z. Zhang, B. Xu, X. Xu, P. He and X. Wang, *J. Am. Chem. Soc.*, 2013, **135**, 18304-18307.
- 110 F. Saleem, B. Xu, B. Ni, H. Liu, F. Nosheen, H. Li and X. Wang, *Adv. Mater.*, 2014, 10.1002-adma.201405319R201405311.
- 111 S. Guo, X. Zhang, W. Zhu, K. He, D. Su, A. Mendoza-Garcia, S. F. Ho, G. Lu and S. Sun, *J. Am. Chem. Soc.*, 2014, **136**, 15026-15033.
- 112 X. Huang, Y. Chen, E. Zhu, Y. Xu, X. Duan and Y. Huang, *J. Mater. Chem. A*, 2013, **1**, 14449-14454.
- 113 C. Wang, D. Van der Vliet, K. L. More, N. J. Zaluzec, S. Peng, S. Sun, H. Daimon, G. Wang, J. Greeley and J. Pearson, *Nano Lett.*, 2010, **11**, 919-926.
- 114 K. Sasaki, H. Naohara, Y. Choi, Y. Cai, W.-F. Chen, P. Liu and R. R. Adzic, *Nat. Comm.*, 2012, **3**, 1115/1111-1115/1119.
- 115 K. Gong, D. Su and R. R. Adzic, *J. Am. Chem. Soc.*, 2010, **132**, 14364-14366.
- 116 H.-L. Jiang and Q. Xu, *J. Mater. Chem.*, 2011, **21**, 13705-13725.
- 117 H. Yang, *Angew. Chem. Int. Ed.*, 2011, **50**, 2674-2676.
- 118 Z. Peng and H. Yang, *Nano Today*, 2009, **4**, 143-164.
- 119 F.-R. Fan, D.-Y. Liu, Y.-F. Wu, S. Duan, Z.-X. Xie, Z.-Y. Jiang and Z.-Q. Tian, *J. Am. Chem. Soc.*, 2008, **130**, 6949-6951.
- 120 V. Mazumder, M. Chi, K. L. More and S. Sun, *J. Am. Chem. Soc.*, 2010, **132**, 7848-7849.
- 121 X. Sun, D. Li, Y. Ding, W. Zhu, S. Guo, Z. L. Wang and S. Sun, *J. Am. Chem. Soc.*, 2014, **136**, 5745-5749.
- 122 S. Zhang, Y. Hao, D. Su, V. V. T. Doan-Nguyen, Y. Wu, J. Li, S. Sun and C. B. Murray, *J. Am. Chem. Soc.*, 2014, **136**, 15921-15924.
- 123 S.-I. Choi, M. Shao, N. Lu, A. Ruditskiy, H.-C. Peng, J. Park, S. Guerrero, J. Wang, M. J. Kim and Y. Xia, *ACS Nano*, 2014, **8**, 10363-10371.
- 124 Y. Kang, L. Qi, M. Li, R. E. Diaz, D. Su, R. R. Adzic, E. Stach, J. Li and C. B. Murray, *ACS Nano*, 2012, **6**, 2818-2825.
- 125 J. Yang, X. Chen, X. Yang and J. Y. Ying, *Energy Environ. Sci.*, 2012, **5**, 8976-8981.
- 126 S. Guo, S. Zhang, D. Su and S. Sun, *J. Am. Chem. Soc.*, 2013, **135**, 13879-13884.
- 127 B. T. Sneed, A. P. Young, D. Jalalpoor, M. C. Golden, S. Mao, Y. Jiang, Y. Wang and C.-K. Tsung, *ACS Nano*, 2014, **8**, 7239-7250.
- 128 S. W. Kang, Y. W. Lee, Y. Park, B.-S. Choi, J. W. Hong, K.-H. Park and S. W. Han, *ACS Nano*, 2013, **7**, 7945-7955.
- 129 R. R. Adzic, J. Zhang, K. Sasaki, M. B. Vukmirovic, M. Shao, J. Wang, A. U. Nilekar, M. Mavrikakis, J. Valerio and F. Uribe, *Topics Catal.*, 2007, **46**, 249-262.
- 130 K. A. Kuttiyiel, K. Sasaki, Y. Choi, D. Su, P. Liu and R. R. Adzic, *Energy Environ. Sci.*, 2012, **5**, 5297-5304.
- 131 Z. Peng, H. You and H. Yang, *Adv. Funct. Mater.*, 2010, **20**, 3734-3741.
- 132 F. Tao, M. E. Grass, Y. Zhang, D. R. Butcher, J. R. Renzas, Z. Liu, J. Y. Chung, B. S. Mun, M. Salmeron and G. A. Somorjai, *Science*, 2008, **322**, 932-934.
- 133 B. Hammer and J. K. Nørskov, in *Adv. Catal.*, ed. H. K. Bruce C. Gates, Academic Press, 2000, vol. Volume 45, pp. 71-129.
- 134 J. Greeley, J. K. Nørskov and M. Mavrikakis, *Annu. Rev. Phys. Chem.*, 2002, **53**, 319-348.
- 135 U. B. Demirci, *J. Power Sources*, 2007, **173**, 11-18.
- 136 C. Solliard and M. Flueli, *Surf. Sci.*, 1985, **156**, 487-494.
- 137 B. Medasani and I. Vasiliev, *Surf. Sci.*, 2009, **603**, 2042-2046.
- 138 J. Kitchin, J. K. Nørskov, M. Barteau and J. Chen, *J. Chem. Phys.*, 2004, **120**, 10240-10246.
- 139 A. Groß, *Topics Catal.*, 2006, **37**, 29-39.
- 140 M. Gsell, P. Jakob and D. Menzel, *Science*, 1998, **280**, 717-720.
- 141 B. T. Sneed, C. N. Brodsky, C.-H. Kuo, L. K. Lamontagne, Y. Jiang, Y. Wang, F. Tao, W. Huang and C.-K. Tsung, *J. Am. Chem. Soc.*, 2013, **135**, 14691-14700.
- 142 C. N. Brodsky, A. P. Young, K. C. Ng, C.-H. Kuo and C.-K. Tsung, *ACS Nano*, 2014, **8**, 9368-9378.
- 143 M. Mavrikakis, B. Hammer and J. K. Nørskov, *Phys. Rev. Lett.*, 1998, **81**, 2819-2822.
- 144 S.-I. Choi, S. Xie, M. Shao, J. H. Odell, N. Lu, H.-C. Peng, L. Protsailo, S. Guerrero, J. Park and X. Xia, *Nano Lett.*, 2013, **13**, 3420-3425.
- 145 J. Yang, J. Yang and J. Y. Ying, *ACS Nano*, 2012, **6**, 9373-9382.
- 146 J. Wu, L. Qi, H. You, A. Gross, J. Li and H. Yang, *J. Am. Chem. Soc.*, 2012, **134**, 11880-11883.
- 147 A.-X. Yin, X.-Q. Min, W. Zhu, H.-S. Wu, Y.-W. Zhang and C.-H. Yan, *Chem. Commun.*, 2012, **48**, 543-545.
- 148 H. You, D. Zurawski, Z. Nagy and R. Yonco, *J. Chem. Phys.*, 1994, **100**, 4699-4702.
- 149 S. Guo, S. Zhang and S. Sun, *Angew. Chem. Int. Ed.*, 2013, **52**, 8526-8544.
- 150 C. Wang, M. Chi, G. Wang, D. Van der Vliet, D. Li, K. More, H. H. Wang, J. A. Schlueter, N. M. Markovic and V. R. Stamenkovic, *Adv. Funct. Mater.*, 2011, **21**, 147-152.
- 151 L. Gan, M. Heggen, S. Rudi and P. Strasser, *Nano Lett.*, 2012, **12**, 5423-5430.
- 152 S. Zhang, X. Zhang, G. Jiang, H. Zhu, S. Guo, D. Su, G. Lu and S. Sun, *J. Am. Chem. Soc.*, 2014, 7734-7739.
- 153 S. Prabhudev, M. Bugnet, C. Bock and G. A. Botton, *ACS Nano*, 2013, **7**, 6103-6110.
- 154 D. Wang, H. L. Xin, R. Hovden, H. Wang, Y. Yu, D. A. Muller, F. J. DiSalvo and H. D. Abruña, *Nat. Mater.*, 2013, **12**, 81-87.
- 155 X. Wang, Y. Orikasa, Y. Takesue, H. Inoue, M. Nakamura, T. Minato, N. Hoshi and Y. Uchimoto, *J. Am. Chem. Soc.*, 2013, **135**, 5938-5941.
- 156 X. Huang, Z. Zhao, J. Fan, Y. Tan and N. Zheng, *J. Am. Chem. Soc.*, 2011, **133**, 4718-4721.
- 157 T. Yu, D. Y. Kim, H. Zhang and Y. Xia, *Angew. Chem. Int. Ed.*, 2011, **50**, 2773-2777.